NASA CONTRACTOR
REPORT

NASA CR-61387

RF MULTICOUPLER DESIGN TECHNIQUES TO MINIMIZE PROBLEMS OF CORONA, MULTIPACTION, AND STABILITY

By Harlan S. Hurley and Dennis J. Kozakoff
Sperry Rand Corporation
Space Support Division
Huntsville, Alabama

December 31, 1971

Prepared for

NASA-GEORGE C. MARSHALL SPACE FLIGHT CENTER
Marshall Space Flight Center, Alabama 35812

TECHNICAL REPORT STANDARD TITLE PAGE

1. REPORT NO.	2. GOVERNMENT ACCESSION NO.	3. RECIPIENT'S CATALOG NO.
NASA CR-61387		

4. TITLE AND SUBTITLE	5. REPORT DATE
RF MULTICOUPLER DESIGN TECHNIQUES TO MINIMIZE PROBLEMS OF CORONA, MULTIPACTION, & INSTABILITY	December 31, 1971
	6. PERFORMING ORGANIZATION CODE
7. AUTHOR(S) Harlan S. Hurley and Dennis J. Kozakoff	8. PERFORMING ORGANIZATION REPORT # SP-273-0566
9. PERFORMING ORGANIZATION NAME AND ADDRESS Sperry Rand Corporation Space Support Division Huntsville, Alabama	10. WORK UNIT NO.
	11. CONTRACT OR GRANT NO. NAS 8-21812-TD 60
12. SPONSORING AGENCY NAME AND ADDRESS National Aeronautics and Space Administration Washington, D. C. 20546	13. TYPE OF REPORT & PERIOD COVERED CONTRACTOR
	14. SPONSORING AGENCY CODE

15. SUPPLEMENTARY NOTES

16. ABSTRACT

While corona breakdown is caused from the ionization of a gas, multipacting breakdown is governed by the phase of the electron motion with respect to the field and by the nature of the wall's materials. Based on experimental results from other authors and equations derived in this report, a mathematical expression was derived describing multipacting and corona effects in a coaxial cavity.

Both mechanical and electrical design techniques were investigated to minimize the susceptibility of a coaxial cavity to corona and multipacting type breakdown. To assist in the design of a multicoupler free from corona and multipactor breakdown, a flow chart obtained from the derived mathematical expression is included.

17. KEY WORDS	18. DISTRIBUTION STATEMENT
RF multicoupler Coaxial cavity Corona Multipaction	Unclassified-unlimited Reginald A. Inman

19. SECURITY CLASSIF. (of this report)	20. SECURITY CLASSIF. (of this page)	21. NO. OF PAGES	22. PRICE
unclassified	Unclassified	88	$3.00

MSFC - Form 3292 (May 1969)

TABLE OF CONTENTS

LIST OF ILLUSTRATIONS

LIST OF TABLES

TABLE OF UNITS

λ = wavelength

v_i = ionization rate (electrons/sec)

v_a = attachment rate (electrons/sec)

v = $v_i - v_a$ = recombination rate (electrons/sec)

Λ = characteristic diffusion length

D = the diffusion coefficient for electrons

E = E field

p = pressure

b = outer radius of a coaxial cavity

a = inter radius of a coaxial cavity

n = electron concentration

V = peak cavity voltage

η = 120π

P = power

Q = loaded Qof the cavity

Q_u = unloaded Q of the cavity

c = speed of light = 3×10^8 meters/second.

f = frequency

fd = minimum fd product where multipacting will not occur

R = A constant which is a function of the b/a ratio

d = (b-a) gap width

δ = secondary emission ratio

δ_s = skin depth

1.0 INTRODUCTION

This study considers the problems of designing multicouplers that are free from the problems of corona, multipaction, and instability. The feasibility, advantages, and disadvantages of design techniques which have been used in the past are included in this study.

The problems of corona discharge exist from sea level down to a pressure of about 10^{-5} Torr. Multipaction discharge, on the other hand, can only occur below a pressure of 10^{-2} Torr, where the gap width is much less than the mean free path of an electron. For rf multicouplers operating at frequencies greater than 200 MHz, the criterion for corona breakdown is determined by the diffusion processes of electrons in the gap created by ionization of gas molecules. For multipacting, electrons emitted by secondary emission at the electrodes take part in an electron resonance phenomena, where both the magnitude of the field and the phase of the electron motion with respect to the electric field are important.

In this study both mechanical and electrical approaches are investigated in order to eliminate the breakdown problems discussed. It is one objective of this study not to repeat the material presented on gaseous breakdown by Rainwater [8], or that on multipacting breakdown by Kozakoff [9], but rather to compliment and tie together those previous studies, showing how the results are applicable to practical multicoupler design problems.

Table 1-1 summarizes various breakdown suppression techniques studied. While it is seen that pressurization or limiting transmitter power will insure neither corona nor multipactor breakdowns, these are not really solutions to the problem. The only two areas that show real promise of solving both corona and multipactor breakdown are in the areas of dielectric loading of the cavities or higher order mode operation. These are discussed in detail in the appropriate sections of this report.

Table 1-1 Summary of Breakdown Suppression Techniques

Technique	Corona	Multipactor
Mechanical Approaches		
A. Pressurization of Cavity	X	X
B. Thick or thin film coatings		X
C. Dielectric loading of cavity	X	X
D. Control of fd product		X
E. Control of center conductor radius	P	
Electrical Approaches		
A. Limit transmitter power	X	P
B. Minimize Q of cavity	P	
C. Minimize Z_o of cavity	P	
D. Application of dc bias		X
E. Higher order mode operation (Non TEM modes)	P	X

X = Breakdown suppression possible

P = Very limited breakdown suppression possible

2.0 CORONA BREAKDOWN

2.1 Ceneral

The term corona refers to a low current gas discharge. In its strictest usage, corona applies to a partial breakdown caused by high fields at one electrode, but no current necessarily bridges the gap between the electrodes. In this case the principal result is a reactive effect on the electrical circuit.

A brief physical description of this phenomena is as follows: if there is a strong electric field, free electrons in the gas near the positive electrode move toward it. The electrons gain energy rapidly from the intense electric field and they produce many free ions in a small volume near the anode. When the ions get sufficiently numerous, a positive streamer moves outward from the electrode. Such streamers give a characteristic brush-like appearance, bright blue in color. If the fields get higher, the streamers propagate further toward the cathode. When they reach the cathode with enough intensity a spark results, followed by a glow, arc, or extinction, depending on the discharge conditions.

The approach taken in the literature to determine corona breakdown thresholds at microwave frequencies is based on the solution of Boltzman's differential equation for the diffusion of electrons in an ionized gas. At high frequency practically none of the electrons generated by corona are collected at the anode; electrons are lost mainly by diffusion to the container walls and electrodes, and by recombination with positive ions. The criterion for breakdown is determined by the balance of the rate of electron generation with the rate of loss by diffusion processes. When the gain of electrons from ionization exceeds the electron losses, breakdown occurs.

A corona discharge can chemically degrade surfaces and raise electrical losses. More often, electrical performance degradation may occur as a result of impedance changes due to the ionized plasma, detuning tuned cavities, heating of surfaces, and possible transition from a corona to a gas discharge type breakdown.

2.2 Design Techniques to Reduce Corona Susceptibility

In the following subsections, electrical and mechanical design approaches are investigated which result in elimination of corona and gas discharge type breakdowns.

2.2.1 Electrical

Suppression of corona or gas breakdown in microwave cavities depends on a good understanding of the electrical phenomena governing breakdown. The analytical approach taken in the literature addresses the problem from the standpoint of diffusion processes of the free electrons liberated by ionization as the result of high electric accelerating fields.

The rate at which the electron concentration is changing is given in terms of the ionization and attachment rates, v_i and v_a, respectively, via

$$\frac{dn}{dt} = \left(v_i - v_a - \frac{D}{\Lambda^2}\right)n \qquad (2\text{-}1)$$

where D is the diffusion coefficient and Λ the characteristic diffusion length. This shows that the rate of change of electron concentration depends on the difference between the rate at which electrons are being produced by ionization of gas atoms by the accelerating electric field minus the rate at which electrons are being lost due to the attachment of electrons to neutral molecules and diffusion of electrons into the walls of the cavity. The process of recombination is another phenomenon whereby free electrons are removed from a discharge, but it has been found that at microwave frequencies recombination is negligible.

Integrating equation (2-1) gives an expression for the total electron concentration

$$n = n_o\, e^{(v_i - v_a - D/\Lambda^2)t} \quad . \qquad (2\text{-}2)$$

When the gain in electron density due to ionization of the gas becomes equal to or exceeds the loss of electrons, a gas discharge occurs. At breakdown

$$\nu_i - \nu_a - D/\Lambda^2 = 0 \qquad (2\text{-}3)$$

or

$$\nu = \nu_a - \nu_i = D/\Lambda^2 \qquad (2\text{-}4)$$

from which we define the breakdown condition as

$$\nu\lambda = D\lambda/\Lambda^2 \quad . \qquad (2\text{-}5)$$

At this point, it is necessary to resort to experimental data to arrive at a numerical solution. In figure 2-1 is plotted experimental data [8] by which $\nu\lambda$ may be evaluated, knowing $E\lambda$ and $p\lambda$. An expression for diffusion coefficient was derived by MacDonald [6]

$$D = \frac{10^4}{p}\left\{29 + 0.9\sqrt{\frac{E\lambda}{(p\lambda)^2 + (35.6)^2}}\right\} \quad . \qquad (2\text{-}6)$$

This can be expressed as

$$\frac{D\lambda}{\Lambda^2} = 10^4\left[\frac{\lambda}{\Lambda}\right]^2 \cdot \frac{1}{p\lambda}\left\{29 + 0.9\sqrt{\frac{E\lambda}{(p\lambda)^2 + (356)^2}}\right\} \quad . \qquad (2\text{-}7)$$

$$= 10^4\left[\frac{\lambda}{\Lambda}\right]^2 \cdot S$$

The equilibrium equation (2-5) is equivalent to

$$\nu\lambda \geq 10^4\left[\frac{\lambda}{\Lambda}\right]^2 \cdot S \quad . \qquad (2\text{-}8)$$

The function S is plotted as a function of $p\lambda$ where $E\lambda$ is taken as a parameter, in figure 2-2. It is obvious that a graphical solution to breakdown may be obtained by superimposing figures 2-1 and 2-2, noting equation (2-7).

However, since the objective is to design multicouplers and other microwave devices which will not breakdown at critical pressure, the need exists only to examine the worst critical breakdown case for which equation (2-5) is an identity. The $p\lambda$ at which the E field at breakdown is at its lowest for a given gap width is approximately $p\lambda = 15$. From figures 2-1 and 2-2

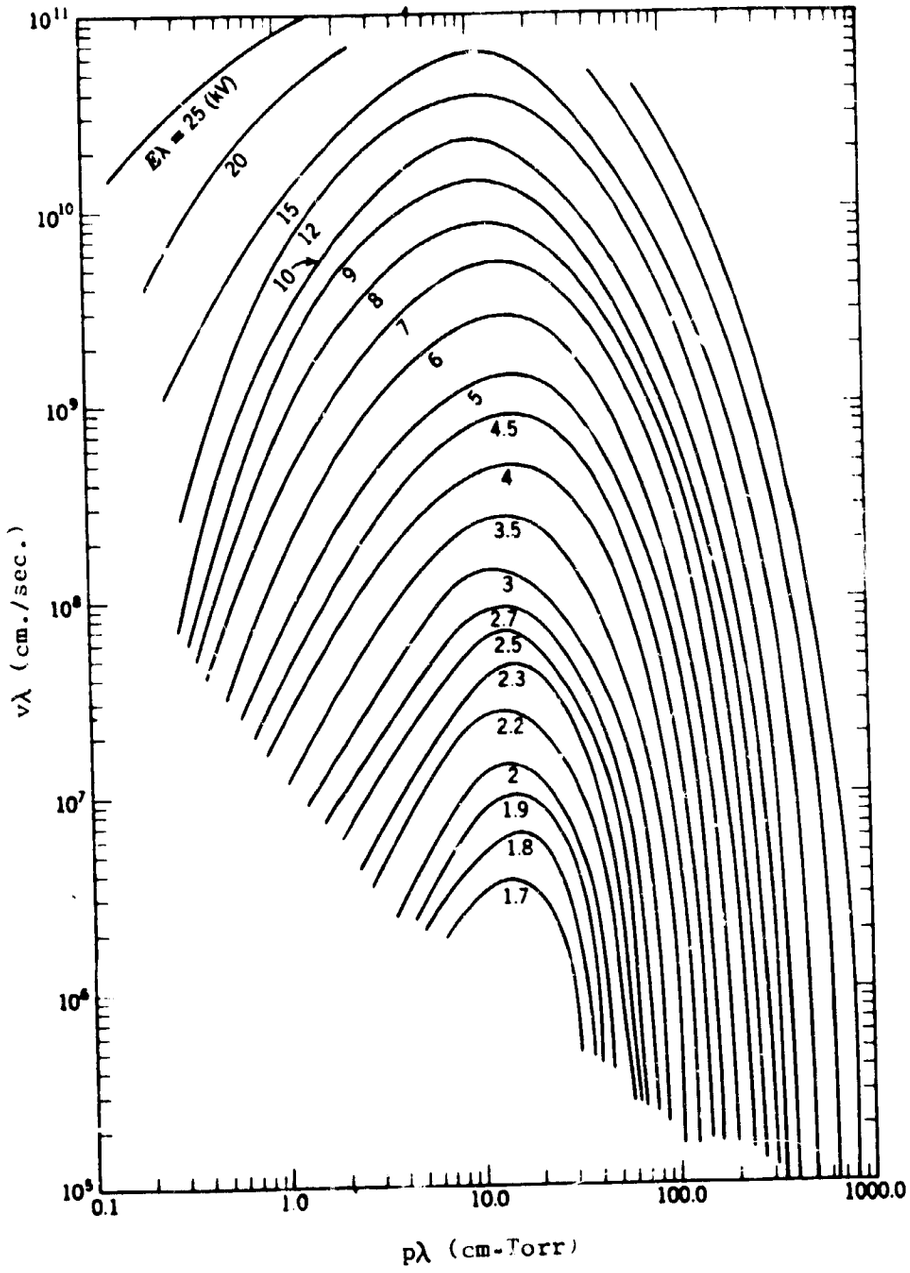

Figure 2-1. vλ plotted as a function of pλ for air, where Eλ is taken as a parameter [8].

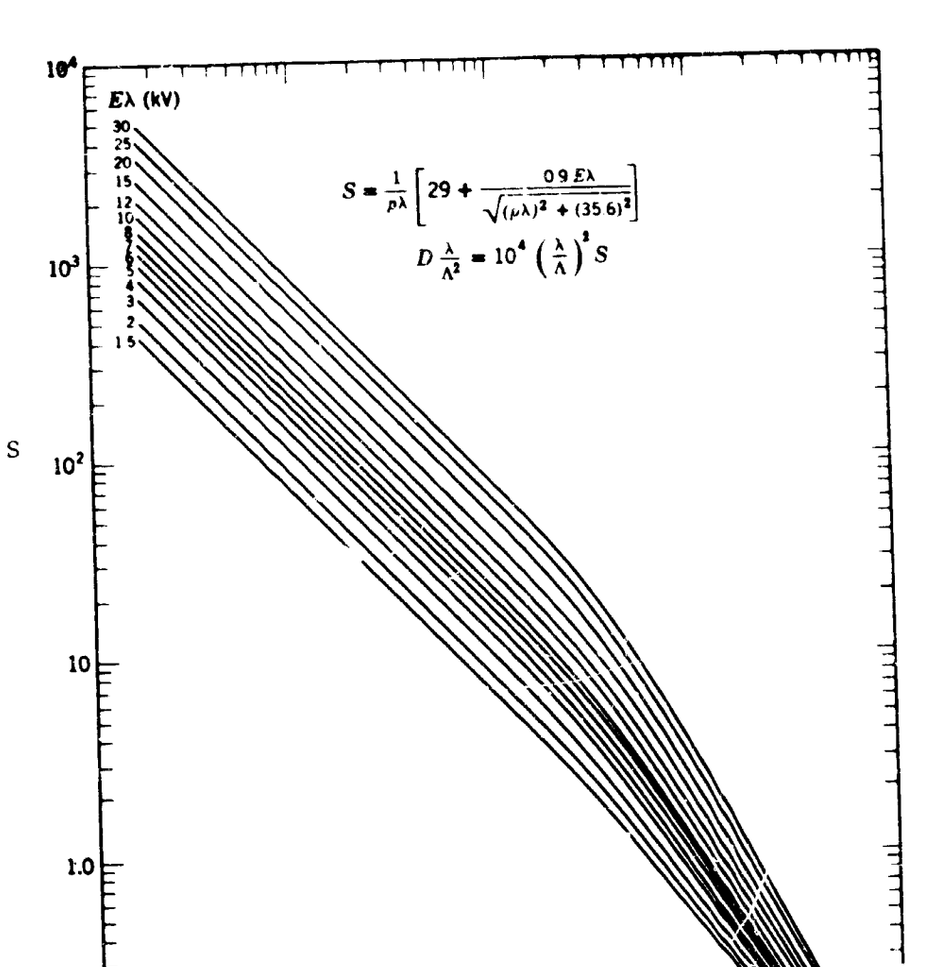

Figure 2-2. The parameter S plotted as a function of pλ, where Eλ is taken as a parameter [6].

a plot of E versus λ/Λ can be obtained for $p\lambda = 15$. A straight line approximation is given by the following equation (E is RMS)

$$E\lambda = 2145.14 + 20\ \lambda/\Lambda \quad . \tag{2-9}$$

For coaxial cavities, from Rainwaters [8] results,

$$\Lambda = \frac{b-a}{R} \quad . \tag{2-10}$$

The diffusion coefficient R is a function of the b/a ratio, but varies over a very limited range over all possible values of (b/a). A good estimate is about 3.1, hence

$$E\lambda = 2145.14 + 62.0\ \frac{\lambda}{b-a} \quad . \tag{2-11}$$

In appendix A an expression for E was derived,

$$E = \frac{V \sin kz}{r \ln (b/a)} \tag{2-12}$$

which has a maximum value of

$$E_{max} = \frac{V}{a \ln(b/a)} \quad . \tag{2-13}$$

From equations (2-11) and (2-13) the maximum peak cavity voltage is

$$V = \frac{3033.08\ a \ln(b/a)}{\lambda} + \frac{\ln (b/a)\ .88}{(b/a - 1)} \tag{2-14}$$

Evaluating this for the case of highest Q, b/a = 3.65, and at VHF (250 MHz) the following relation is found which is plotted in figure 2-3

$$V = 33.23\ a + 41.86 \quad . \tag{2-15}$$

Using the relation derived in appendix A, this can also be expressed in terms of power as shown in figure 2-4. S-band computations of breakdown voltage and power as a function of center conductor radius as shown in figures 2-5 and 2-6, respectively.

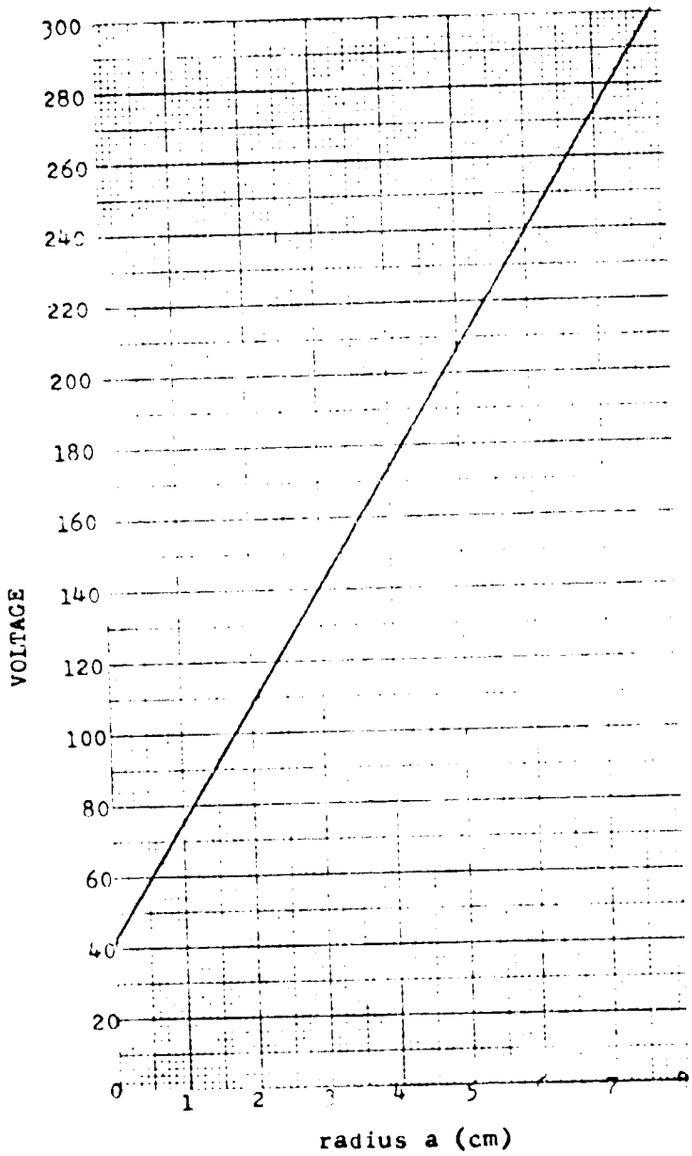

Figure 2-3. Breakdown cavity voltage as a function of center conductor radius at critical pressure. (250 MHz)

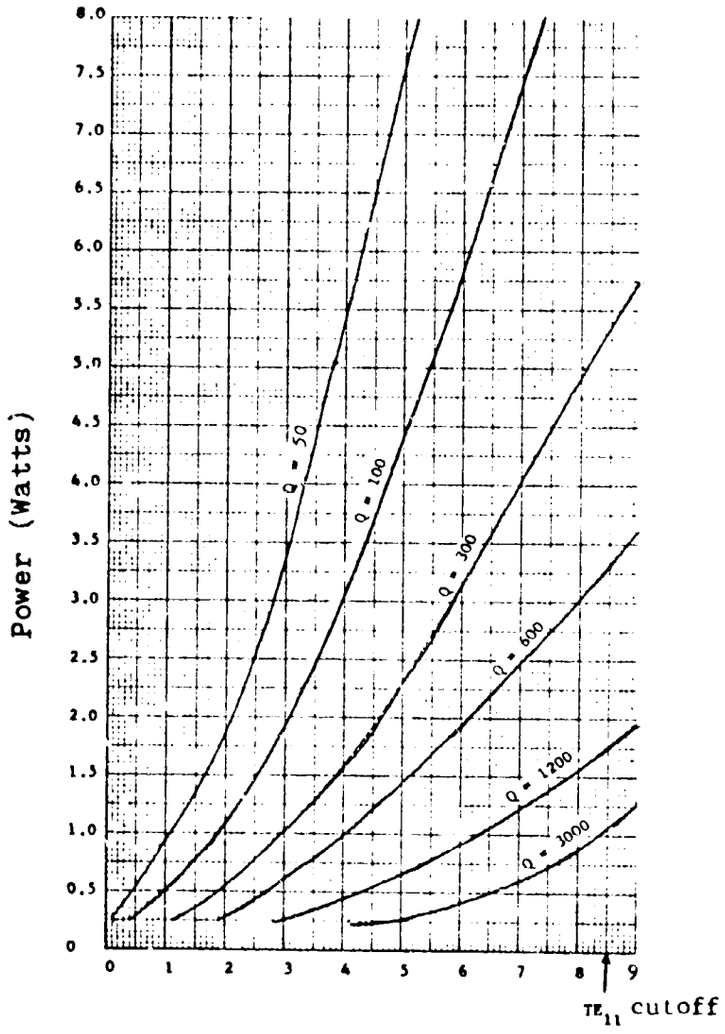

Figure 2-4. Breakdown cavity power at critical pressure versus center conductor radius, where loaded Q is taken as a parameter. (250 MHz)

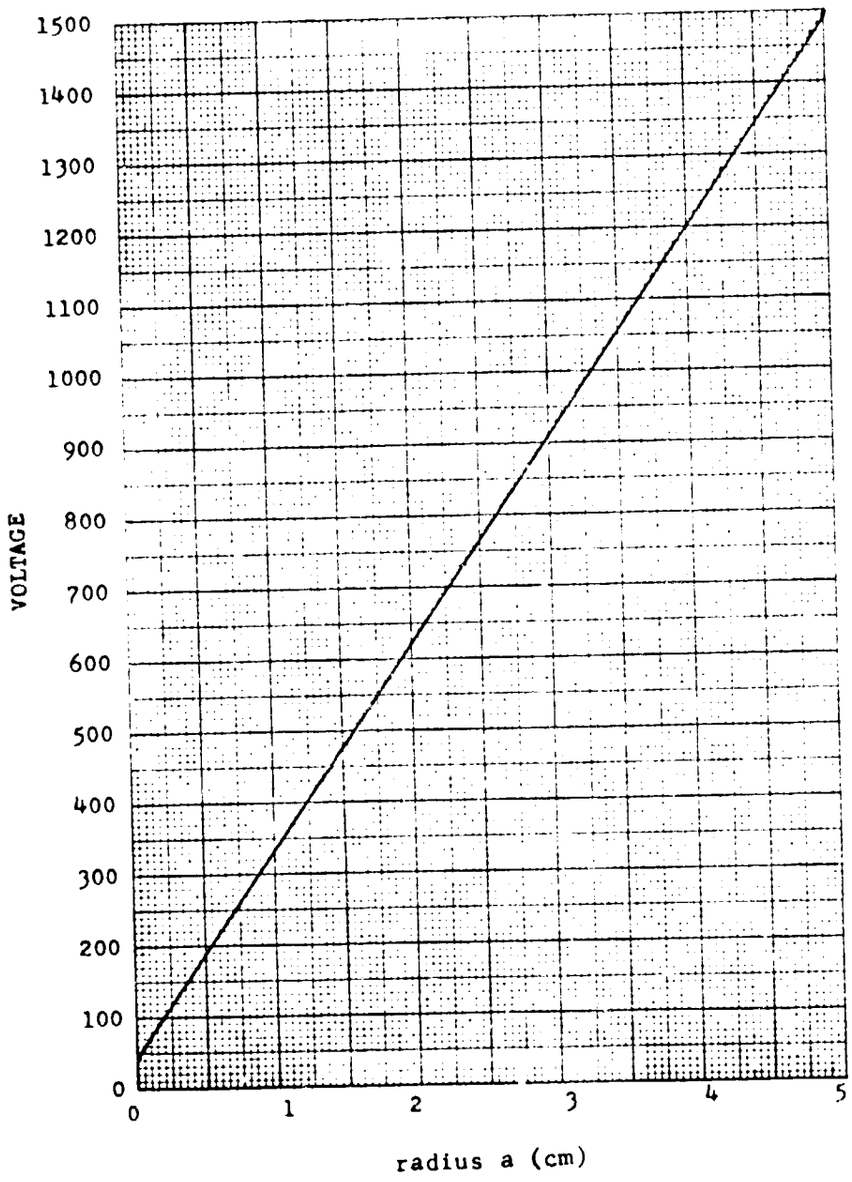

Figure 2-5. Breakdown cavity voltage as a function of center conductor radius at critical pressure. (2.3 GHz)

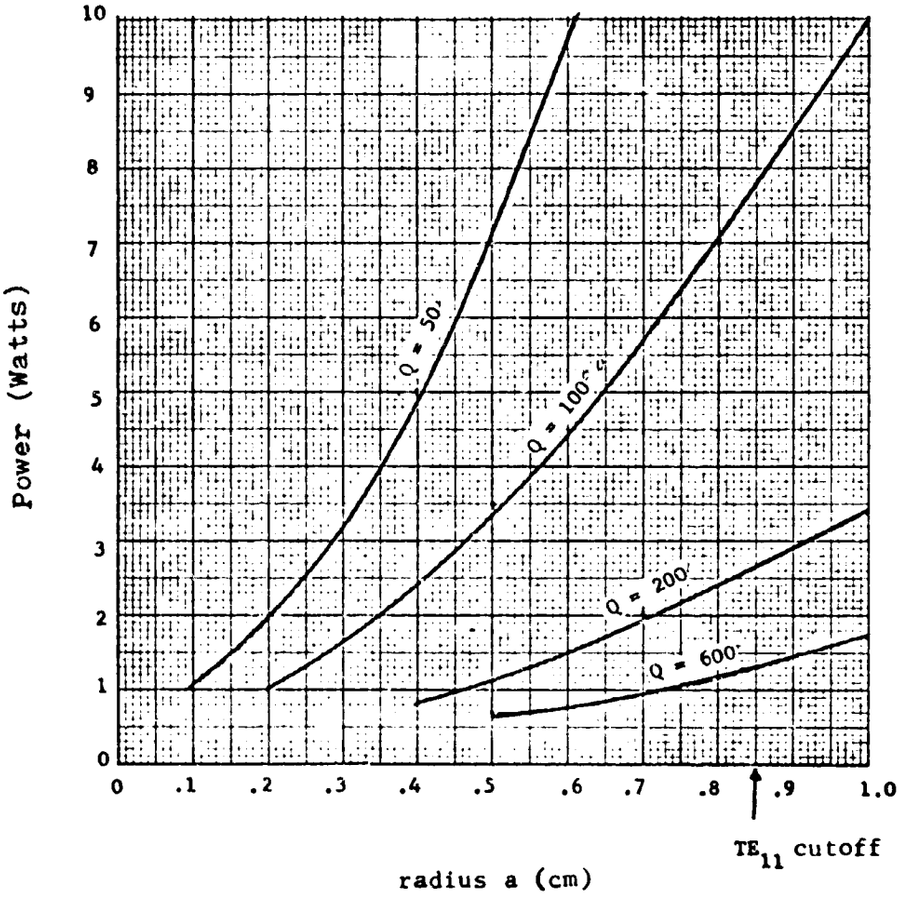

Figure 2-6. Breakdown cavity power at critical pressure versus center conductor radius, where loaded Q is taken as a parameter. (2.3 GHz)

2.2.2 Mechanical

Since points of sharp edges produce high electric fields in the vicinity, they should be avoided at the mechanical design phase. To illustrate, consider a rounded electrode with a 1 cm radius of curvature with applied potentials such that the electrical field near the electrode is 200 volts/cm. If the position is kept fixed and the radius of a curvature is reduced to 1 mm, the electric field becomes 20 000 volts/cm without any change in applied voltage.

The electrical analysis presented prior and in appendices A and B suggests use of low Q and mechanically large structures to lower electric field strengths for a required power handling capability. As such, this implies small (b/a) ratios, and large a.

2.3 Conclusions

Good engineering practice suggests that smooth surfaces and elimination of all sharp edges and points is a first design step toward elimination of corona breakdown problems.

For unvented multicouplers which are required to function at critical pressure, there are several options to maximize power handling capability. First, all radii should be maximized in accordance with figures 2-4 and 2-6. Secondly, since lower Q cavities have higher breakdown power levels than high Q cavities, low Q sections may be cascaded to obtain a desired higher Q while maintaining the high breakdown power level of the single low Q section. The total Q of N cascaded filter sections is related to the Q of a single section via the formula

$$Q_t = \frac{Q}{\sqrt{2^{1/N} - 1}} \qquad (2\text{-}16)$$

where Q is the loaded Q of a single section. The function Q_t/Q is plotted as a function of N in figure 2-7. The practical limit to the number of sections which can be cascaded is determined on the basis of the insertion loss of each individual section and the total insertion loss which can be tolerated in the system.

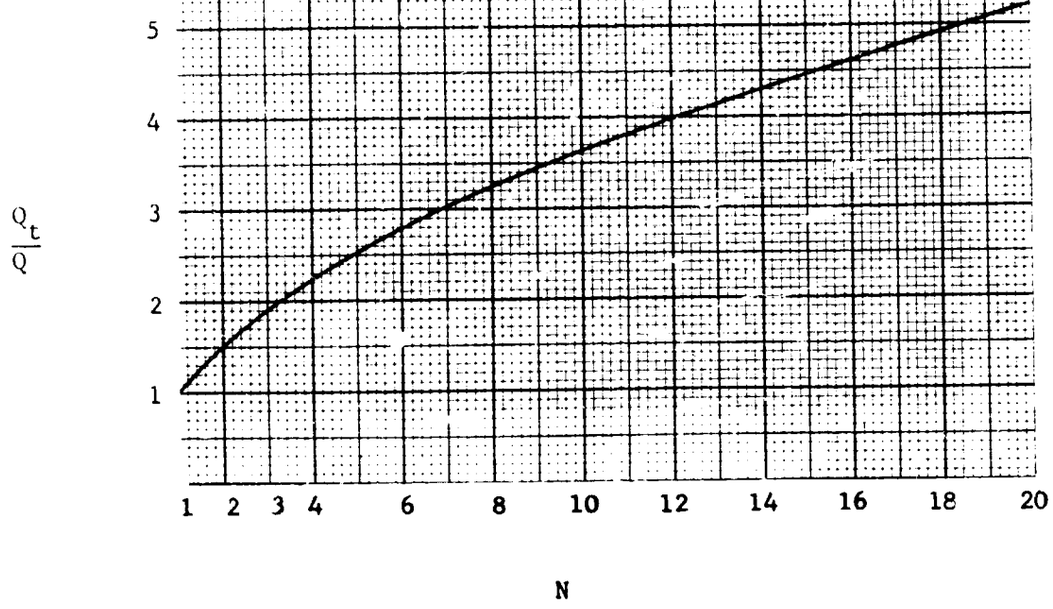

Figure 2-7. Equivalent Q of N cascaded filter sections.

3.0 MULTIPACTOR BREAKDOWN

3.1 General

In a multipactor breakdown, secondary electrons produced at one surface are accelerated across to another in a half cycle of the applied rf field. Upon striking the electrode new secondary electrons are created which are accelerated back across the gap during the next half cycle. Multipacting breakdown is a function of the voltage rather than a function of the field strength, as is the case in gas breakdown. In addition, multipacting breakdown is governed by the phase of the electron motion with respect to the field and by the nature of the wall materials since the electron production depends on secondary emission.

The pressure at which a multipacting discharge can occur is not important as long as the electron mean free path is large compared to the dimensions of the rf system; generally this will occur below 10^{-2} Torr.

Although a multipacting discharge is a fairly high impedance type discharge, the electrical effects on high Q microwave cavities can result in significant change in VSWR as well as detuning. Furthermore, localized heating can produce outgassing and resultant transition to the more serious gas discharge which is a low impedance type discharge.

3.2 Design Techniques to Reduce Multipactor Susceptibility

3.2.1 Mechanical

Certain mechanical parameters enter into the multipactor resonance such as the geometry of the multicoupler or microwave cavity. Also, the conditions for secondary emission from the surfaces are governed by the material, surface conditions, and voltage. In the following subsections design approaches are investigated which suppress multipactor breakdown on the basis of control of important physical parameters of the design.

3.1.1 Control of "fd" Product

Multipactor resonance occurs when the electron transit time is coincident with the applied rf field, or one of its harmonics. A theoretical plot of breakdown voltage versus fd for the parallel plate case is shown in figure 3-1, where the three lowest order multipacting mode regions are indicated. Woo [11] has shown the minimum breakdown voltage for the coaxial case to be higher in general than for the parallel plate case, and specifically, gives results essentially identical when the inner to outer conductor spacing is very small.

Woo's results are valuable since they permit the use of the parallel plate data of figure 3-1 to obtain a lower limit on multipacting voltage for coaxial cavities. If spacing d is interpreted to be the difference between outer and inner radii, (b-a), then a defined lower bound on multipactor susceptibility voltage for coaxial cavities can be plotted as is also shown in figure 3-1.

The equation for this voltage in terms of the frequency-gap spacing product is given by

$$f \cdot (b-a) = 0.894\ V^{1.176} \qquad (3\text{-}1)$$

where f is in MHz and b and a are in centimeters. At rf operating voltages below this voltage, multipacting cannot occur.

In appendix A an expression relating peak cavity voltage to cavity geometry and electrical parameters is derived. That is,

$$V = \sqrt{\frac{2Q\eta P \ln (b/a)}{\pi^2}} \qquad (3\text{-}2)$$

where P is the operating power level, (b/a) the outer to inner radius ratio, and Q the loaded Q of the cavity. A computer program was written (appendix C) incorporating equations (3-1) and (3-2) to relate multicoupler breakdown power level to minimum f·(b-a) product. That is, for an f·(b-a) ratio equal to or greater than the computed values, multipacting cannot occur. This

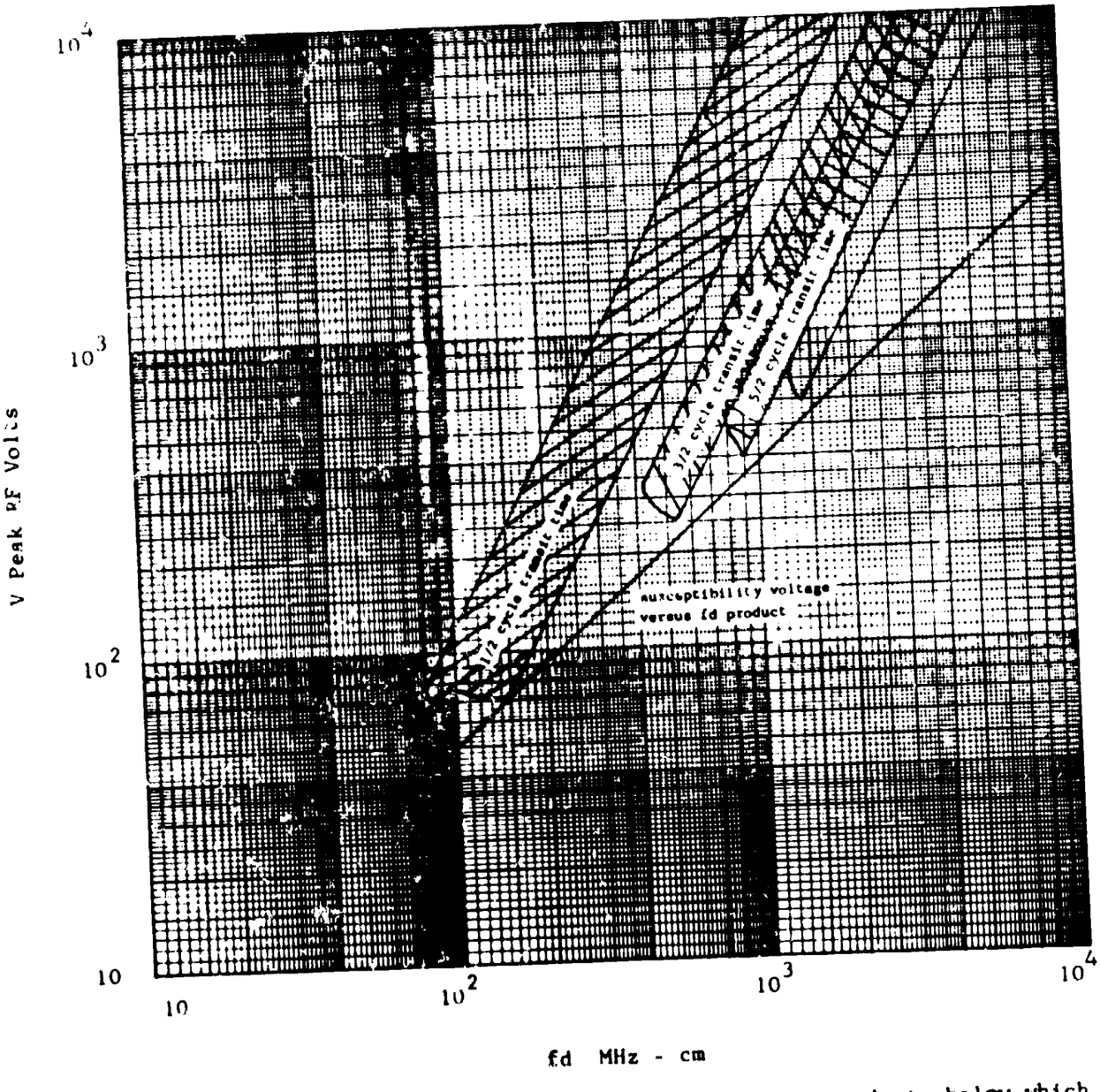

Figure 3-1. A defined minimum breakdown voltage versus fd product, below which multipacting cannot occur (d is gap spacing).

data is plotted in figures 3-2 through 3-4 for (b/a) ratios of 1.65, 2.72, and 3.5, respectively. The reason why these (b/a) ratios were selected for computation is illustrated in figure 3-5, where it is shown that a (b/a) ratio of 1.65 results in a coaxial cavity with highest power handling capability, a (b/a) ratio of 2.72 results in highest internal voltage (actually a worst case), and finally, a (b/a) ratio of 3.5 will result in a cavity of lowest internal losses, and hence, highest Q.

3.2.1.2 Control of Secondary Emission

One method of suppressing multipacting is to employ surfaces which have secondary emission coefficients less than unity. Also, the secondary emission ratio of metal surfaces may be spoiled by use of dielectric coatings or by choice of plating metals with low secondary emission ratios. The maximum secondary emission coefficients and the energy of the incident electrons in electron volts at which the maximum coefficient of secondary emission appears are shown in table 3-1 for a number of elements. In this table, V_p^I and V_p^{II} are respectively, the lower and higher voltage for which the coefficient of secondary emission is equal to one.

What is interesting from this table is that although many metals have maximum coefficients of secondary emission much greater than unity, operating at voltages less than V_p^I multipacting cannot be supported on the basis of secondary emission. For instance, for copper, V_p^I = 220 volts. Thus, below this voltage multipacting cannot occur because the secondary emission coefficient is less than unity.

Seemingly this would offer one solution to the multipacting problem. However, maintaining a pure metal surface finish is difficult since the rapid formation of the metal oxides and other surface contaminations rapidly occurs, which increases the coefficient of secondary emission. Table 3-2 illustrates coefficients of secondary electron emission for some compounds. As is typical of compounds, it is found that, in general, metallic oxides have much higher coefficients than the pure metal. Note comparative values of aluminum oxide and aluminum in the two tables. This means that any oxidation of a surface will tend to make multipacting more likely, an

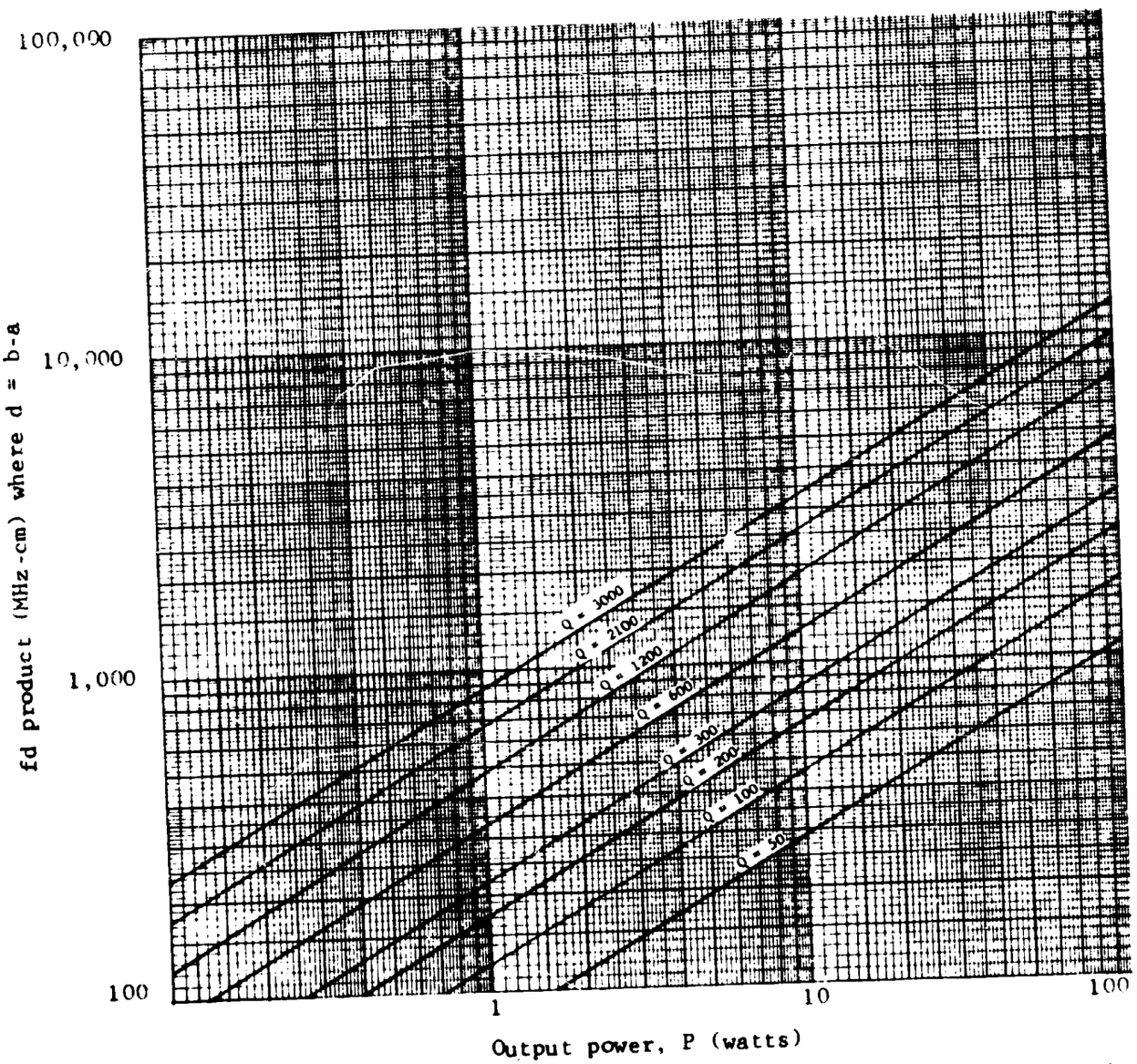

Figure 3-2. Minimum fd product to prevent multipacting versus output power for b/a = 1.65, where Q is taken as a parameter.

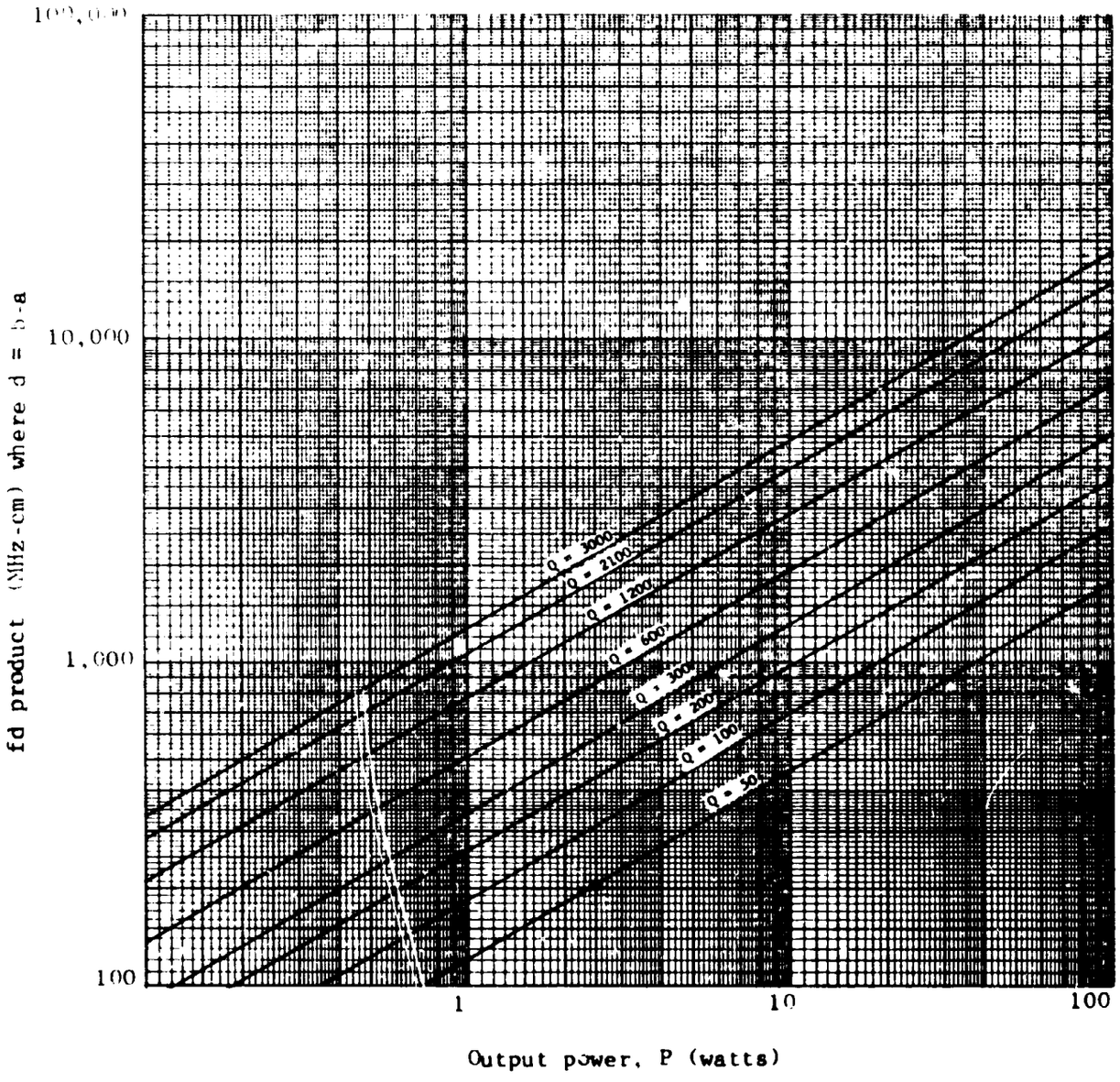

Figure 3-3. Minimum fd product to prevent multipacting versus output power for b/a = 2.72, where Q is taken as a parameter.

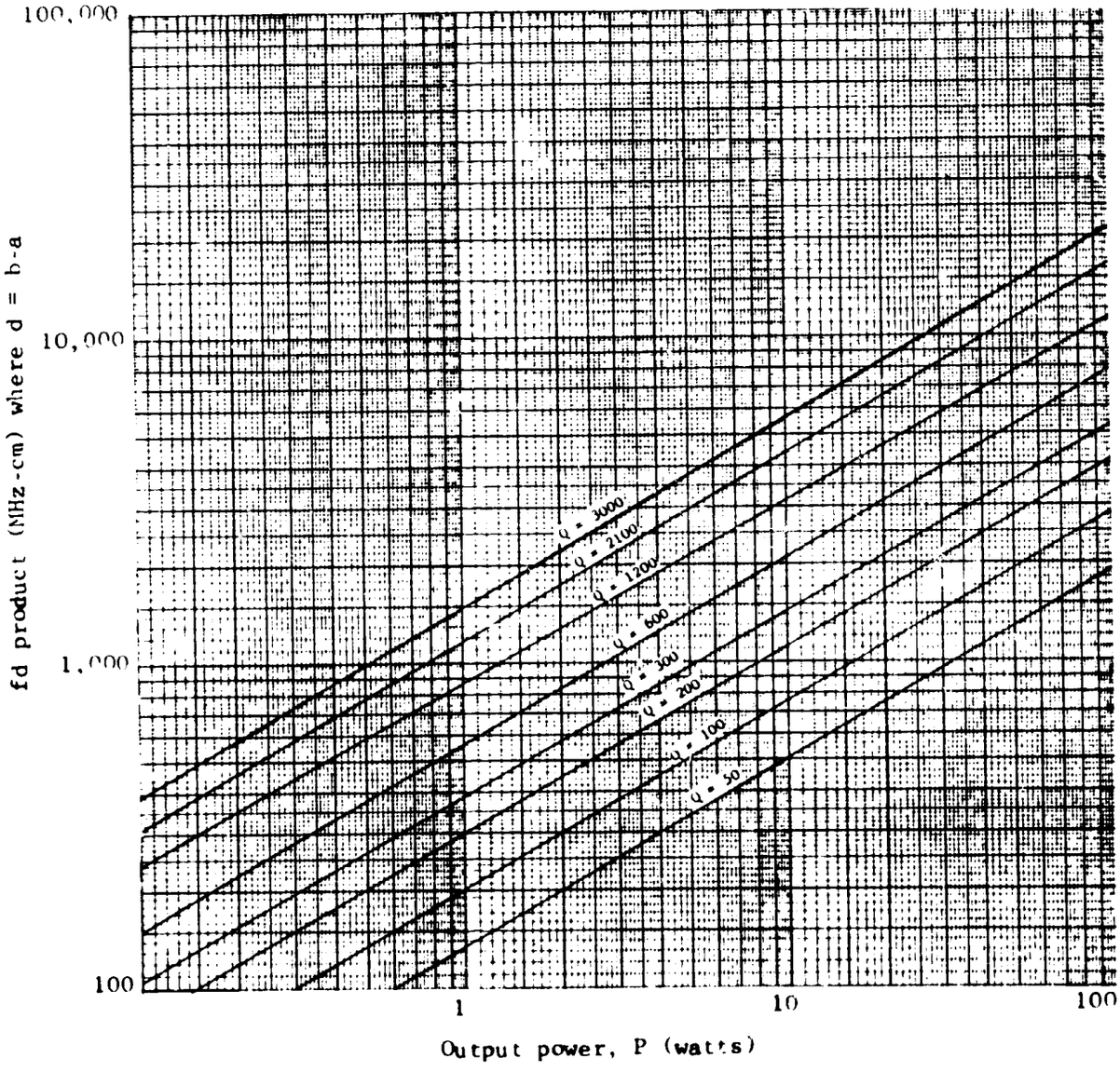

Figure 3-4. Minimum fd product to prevent multipacting versus output power for b/a = 3.5, where Q is taken as a parameter.

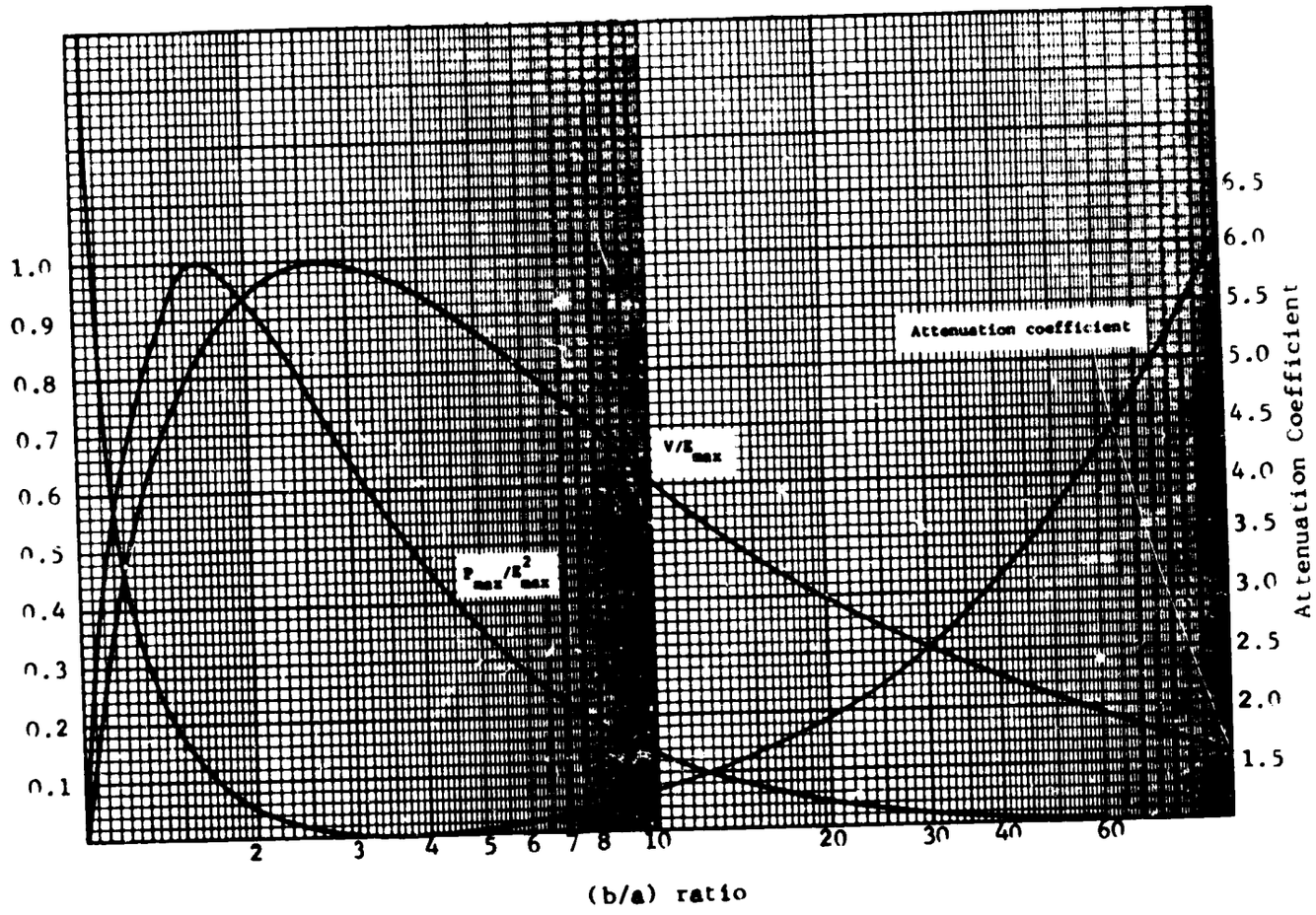

Figure 3-5. Plot of important coaxial line parameters as a function of (b/a) ratio [2].

Table 3-1. Maximum Secondary Electron Emission Yield δ max, and Corresponding $V_{p(max)}$, for Different Elements [4]

Element	δ_{max}	$V_{p\ (max)}$	V_p^{I}	V_p^{II}
Ag	1.5	800	100	-
Al	1.0	300	-	-
Au	1.46	750	100	-
B	1.2	150	80	350
Ba	0.83	400	-	-
Bi	1.15	550	200	1600
Be	0.53	200	-	-
C	1.0	300	250	275
Cd	1.1	400	300	700
Co	1.2	700	300	-
Cs	0.72	400	-	-
Cu	1.3	600	220	-
Fe	1.3	350	100	1400
Ge	1.2	400	150	1300
K	0.75	200	-	-
Li	0.5	85	-	-
Mg	0.95	300	-	-
Mo	1.25	375	150	1350
Nb	1.2	375	150	1100
Ni	1.3	550	150	1700
Pb	1.1	500	250	1000
Pd	1.3*	250*	125	-
Pt	1.8	800	175	-
Rb	0.9	350	-	-
Si	1.1	250	90	700
Sn	1.35	500	180	-
Ti	0.9	280	-	-
W	1.4	700	200	-
Zr	1.1	350	180	-

* $\delta = 1.3$ at $V_p = 250$ V is not maximum value of δ.

Table 3-2. Maximum Yields From Some Metal Compounds [4]

Metal Compounds	δ_{max}	$V_{p\ max}$ (V)	V_f^I (V)	V_f^{II} (V)
LiF	5.6		21	
NaF	5.7		20	
NaCl	6.8		15	
NaCl	6	600		
KCl	7.5		15	
RbCl	5.8			
CsCl	6.5			
NaBr	5.5			
KI	5.5		12	
Cr_3O*	2.3 to 11			
$SbCr_3$	5 to 8.3	375 450	10 20	
CaF_2	3.2			
BaF_2	4.5			
BeO	3.4	2000		
MgO	2.4	1500		
MoO	4.0	400		
BaO	2.3	1600		
PbO	4.8	400		
CaO	2.2	500		
Al_2O_3	1.5 to 4.8	350 to 1300		
mica	2.4	380	30	3300
SiO_2 (quartz)	2.1 to 2.9	400 to 440	30 50	2300
Ag_2O	0.98 to 1.19			
MoS_2	1.10			
MoO_2	1.00 to 1.33			
WO_2	0.96 to 1.04			
Cu_2O	1.10 to 1.25			

important consideration in practical devices that may be exposed to oxygen before use in a vacuum. Also, organic deposits such as oil on a surface tend to reduce the minimum threshold voltage sharply. For instance, recent data indicates the breakdown voltage for a gold surface was reduced from 180 volts to approximately 23 volts when an oil film was deposited on the surface.

If the surface cleanliness of the parts can be maintained, and cavities pressurized with an inert gas to prevent contamination of pure metal, minimum susceptibility to multipacting will be experienced. If the inert gas leaked out in a space vacuum, it would not be a problem since its only purpose was to prevent atmospheric leakage into the cavity, with resulting surface contamination, while at sea level.

Plating cavity walls with pure metals or compounds with coefficients of secondary emmissions less than unity seems a credible approach; however, these may have poor electrical conductivity at microwave frequencies. This will not be a problem if the coating or plating thickness is much less than a skin depth at the rf frequency.

The film thickness necessary for the suppression of multipacting is dependent on the penetration depth of electrons involved in the discharge. At microwave frequencies the penetration will be small since maximum energy gained by an electron accelerated in an rf field is limited to that gained in one-half cycle. Thus, a film of a few hundred angstroms should be thick enough to suppress secondaries at the power levels of interest. To illustrate the order of magnitude of skin depth of common metals, a few are plotted in figure 3-6.

A lamp black coating was used successfully by Nanevicz and Vance to prevent multipacting. The use of carbon and lamp black was rejected because of the difficulty of obtaining and maintaining the thin films necessary to keep the rf losses to an acceptable level, together with the possibility that such thin films would be hard to control in an oxidizing atmosphere.

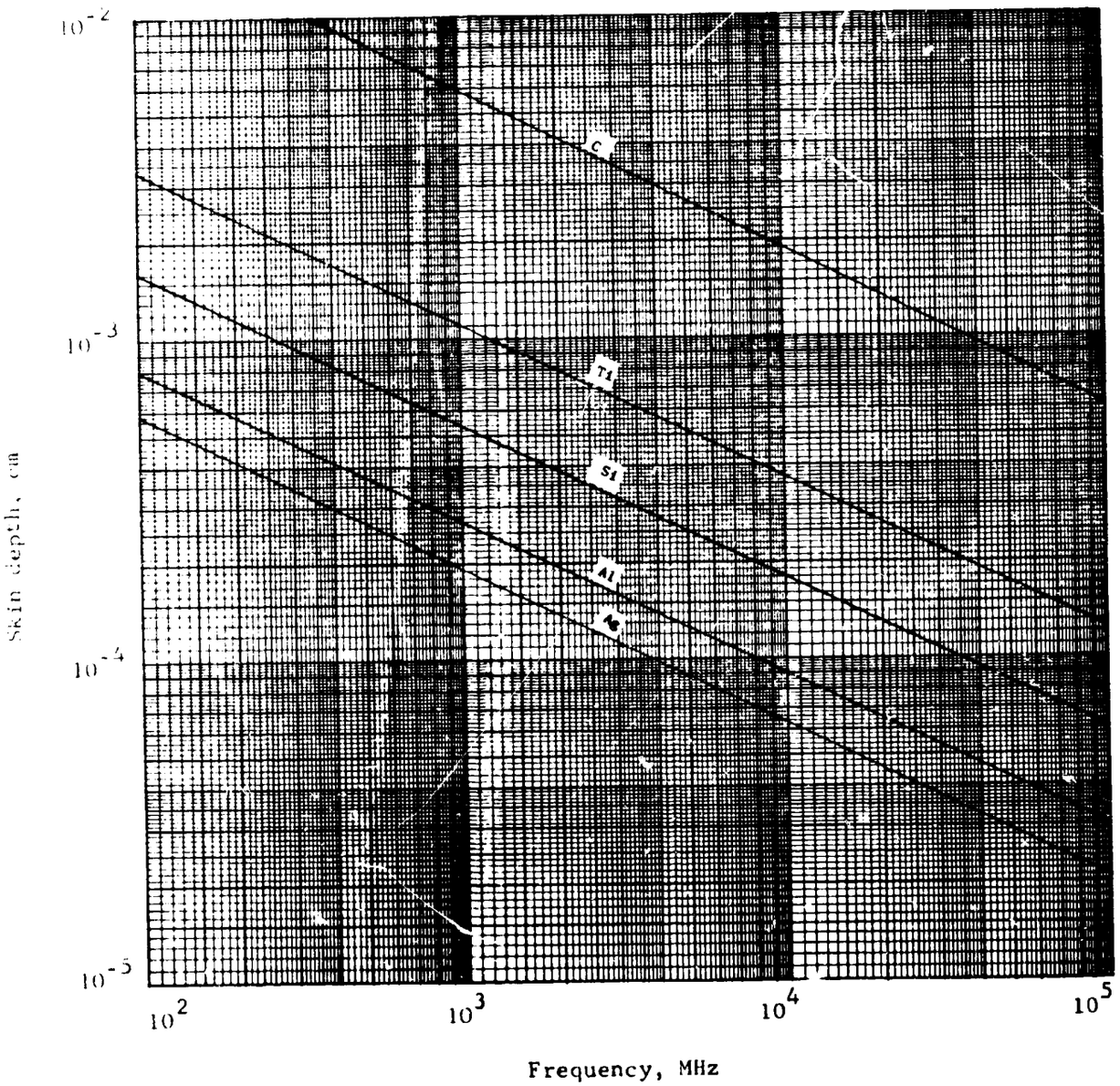

Figure 3-6. Skin depth as a function of frequency for a few common metals [1].

It was found that multipacting can be eliminated by coating the window of a waveguide surface by evaporating titanium in a vacuum or sputtering titanium monoxide in an argon or mercury atmosphere. This process was found satisfactory on waveguide windows. It is not known if the titanium monoxide can be successfully used for gap width and voltage of the magnitude which is present in a coaxial cavity. Presently, there is insufficient information available to determine what compounds, and under what circumstances, they will or will not support a multipacting discharge.

3.2.1.3 Potting or Foaming

In order to establish a multipactor discharge, the mean free path of an electron must be long enough to permit the electron to be accelerated between the two surfaces with a low probability of collision with ambient atoms or molecules. Potting or foaming can reduce mean free path lengths to negligible values, thus preventing multipacting.

Great care must be taken when applying potting or foaming compounds to make sure that no voids are formed which are larger than the mean free path of the electrons in the voids. Failure to eliminate these voids in the compound may cause a corona discharge in the void. This discharge will lead to both physical and chemical deterioration, with ultimate electrical breakdown.

Since the dissipation factor or loss tangent of potting or foaming compound is higher than air, the Q of the cavity is changed. Therefore, when a cavity is foamed or potted, the complete circuit must be returned. The use of foam potting in high-voltage equipment is not recommended. The reason for this is there is no way to predict how long the outgassing of a foam will take. So when high voltages are applied, a corona discharge occurs. In general, the harder the material the less likely a corona discharge will occur. Potting compound, being a harder material, is therefore more satisfactory. Polyurethane, silicone rubber, and epoxy resins are frequently used as potting compounds.

3.2.2 Electrical Design

3.2.2.1 Application of DC Bias

If a dc voltage, in addition to the rf voltage, is applied to the multipactor discharge gap, the electron transit time will be shorter in one direction and longer in the opposite direction. It has been demonstrated that in addition to the two-sided modes in which the electron crosses the gap and strikes the opposite electrode, there exists a one-sided mode in which the electron is carried away from the positive electrode by the rf field when the rf and dc fields are opposing and driven back to the electrode from which it was emitted during the next half cycle when the rf field aids the dc field. By raising the bias enough to cause a significant difference in transit times, it is possible to prevent either a stable single-or double-sided multipacting discharge. By considering the phase stability of the discharge, the amount of bias needed to eliminate multipacting is given in the following equations:

for the n = 1 (½ cycle) multipactor mode

$$V_{dc} = \frac{0.34}{\pi} \frac{(\omega d)^2}{(e/m)} \quad , \tag{3-3}$$

for the n = 3 (3/2 cycle) multipactor mode

$$V_{dc} = \frac{0.12}{\pi} \frac{(\omega d)^2}{(e/m)} \quad , \tag{3-4}$$

and for the n = 5 (5/2 cycle) multipacting mode

$$V_{dc} = \frac{0.07}{\pi} \frac{(\omega d)^2}{(e/m)} \quad . \tag{3-5}$$

This information is shown in figure 3-7 where A is the dc bias voltage needed to suppress multipacting for mode 1. B and C are the dc bias voltages required to suppress multipacting in modes 3 and 5 respectively. Note that the dc bias required to suppress the n = 1 mode will be adequate to suppress all higher modes.

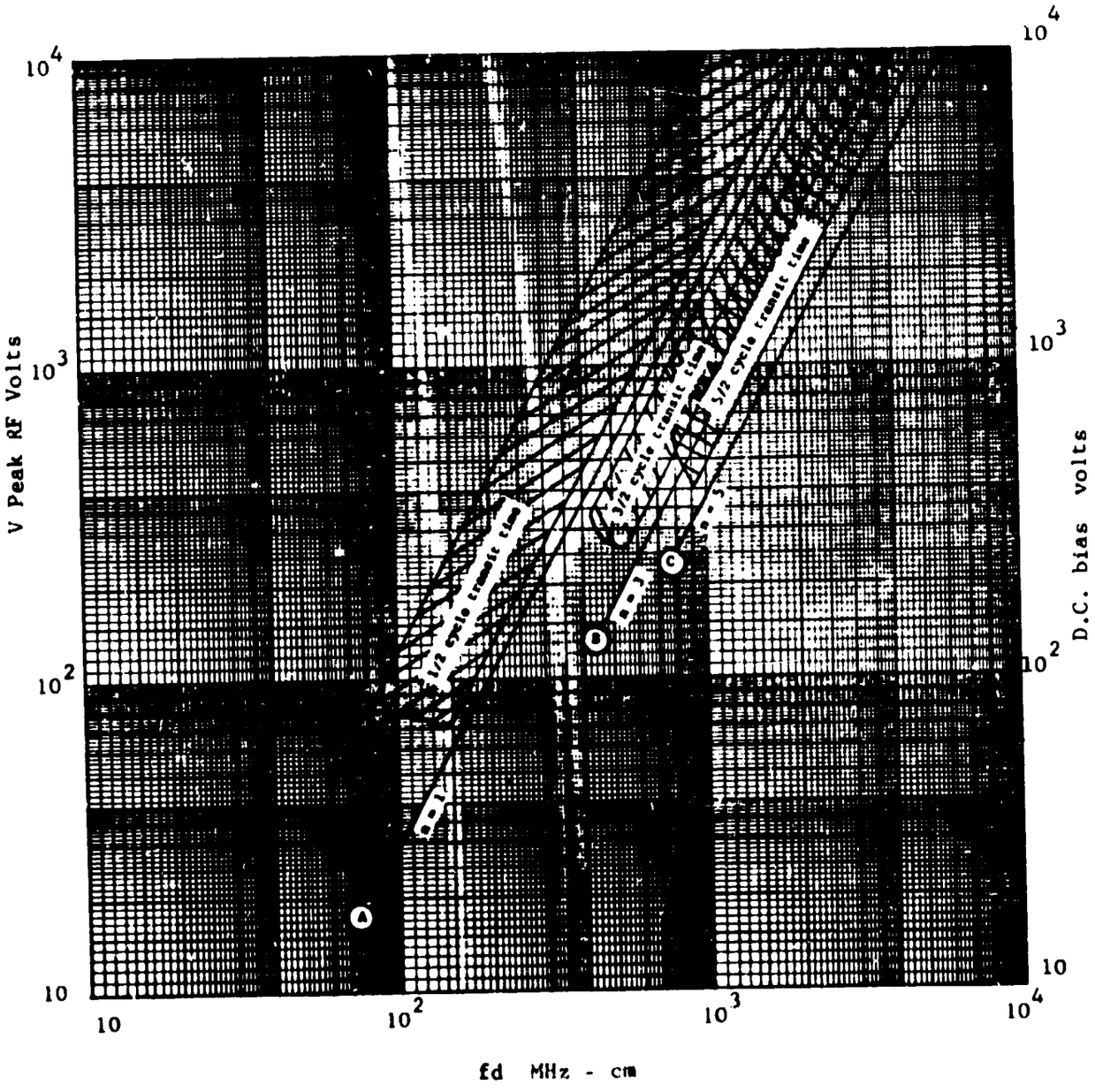

Figure 3-7. Minimum dc bias versus fd product to suppress multipacting modes between parallel plate electrodes (curves A, B & C suppress the n=1, 3 & 5 modes, respectively).

For coaxial electrodes, the effect of the nonuniformity of the electric field is to slow down electrons traveling in the inward radial direction between the coaxial electrodes and to hasten the electrons traveling in the outward radial direction. Application of a small positive dc voltage to the electrodes produces the reverse effect. With an increase in dc voltage the effective b/a ratio is therefore reduced, and from the results brought out in the preceding paragraphs, the rf breakdown voltage would decrease. The effect of dc bias on a coaxial multipactor is illustrated in figure 3-8.

In that figure an expected decrease in rf breakdown voltage is seen going from A to B. If the dc voltage is further increased, a nonuniform situation is created, whereby electrons traveling in the inward radial direction are hastened and electrons traveling in the outward radial direction are slowed down. Between B and C, the rf breakdown voltage will, therefore, increase with an increase in dc voltage. At C the dc voltage is high enough to prevent electrons from reaching the outer electrode, and one-sided multipacting against the inner electrode results. The fact that this multipacting mode occurs was confirmed by replacing the outer electrode with a mesh electrode. At D the multipacting mode returns to the two-sided mode.

Arguments similar to those above explain the increase and decrease of rf breakdown voltage when a negative dc voltage is added. Similar results were obtained with other b/a cases. Because of this property of the discharge, the use of dc bias to prevent multipactor discharges requires careful consideration, since insufficient bias, or partial failure of the bias system, can result in a lower rf breakdown voltage than would be obtained in the absence of bias. Also, its effect on the circuit elements should be considered. Because the one-sided discharge is predominantly reactive (in the uniform field case), the reactive loading associated with the discharge can detune resonant rf circuits, thereby seriously degrading the performance of the rf system.

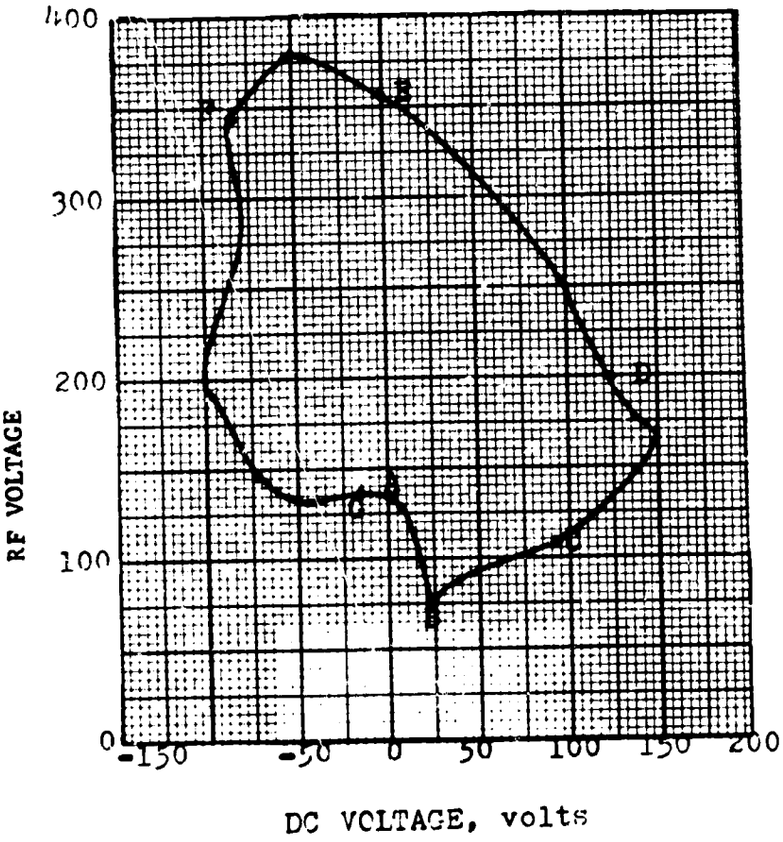

Figure 3-8. Multipacting in the presence of a dc voltage for coaxial electrodes with b/a = 9.13 [11].

3.2.2.2 Control of Peak Voltage

An equation for the multipacting breakdown voltage derived by Hughes Aircraft [10] is given by

$$V = \frac{(2\pi)^2 (fd)^2}{(e/m)} \left[\frac{1}{\frac{K-1}{K+1} \pi \cos \phi + 2 \sin \phi} \right] \qquad (3\text{-}6)$$

where the parameters K and ϕ are determined by experimental observation for a discharge. Specifically,

K = ratio of electron velocity as it strikes electrode to normal velocity component of secondary electrons.

It is seen from the resonance equation that breakdown voltage is closely a function of the fd product. Figure 3-1 gives the minimum rf voltage versus fd product below which multipacting cannot occur. From the previous section on the control of fd product and Appendix A, the peak rf voltage in the coaxial cavity can be found for a given power, b/a ratio, and loaded cavity Q. This information is given in figures 3-9, 3-10 and 3-11. For a given fd product this voltage (V) is found by

$$V = 1.1186 \, (fd)^{.850} \quad . \qquad (3\text{-}7)$$

3.3 Conclusions

Although thick and thin film coatings, potting, foaming, and dc bias are shown to be credible approaches to suppressing multipactor resonance, control of cavity geometry is found to be the best approach. The minimum fd product to prevent multipactor for an expected peak cavity voltage is given by equation (3-1). This voltage is evaluated in terms of cavity power and Q in figures 3-9 through 3-11.

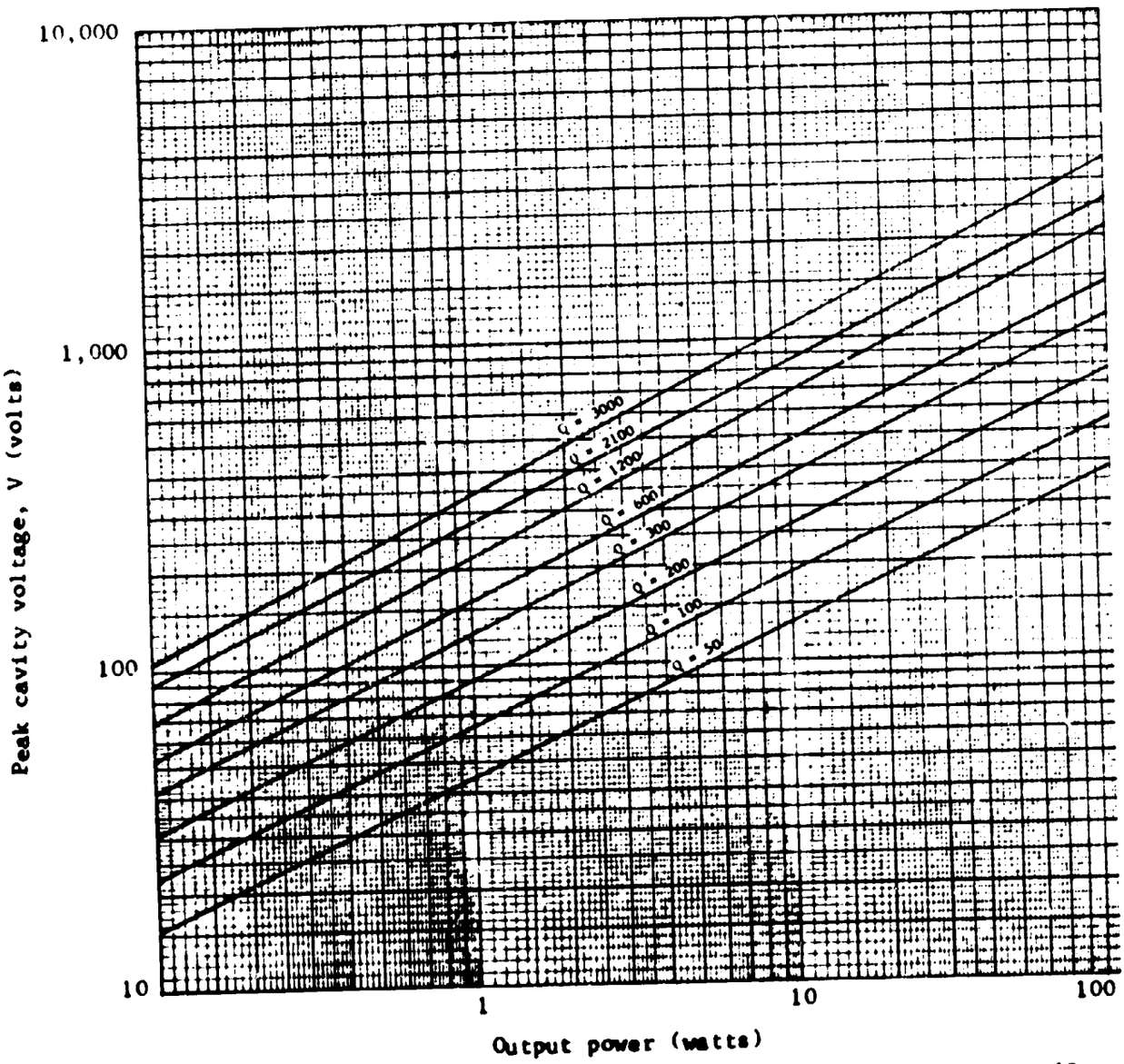

Figure 3-9. Peak cavity voltage versus output power for b/a = 1.65, where loaded Q is taken as a parameter.

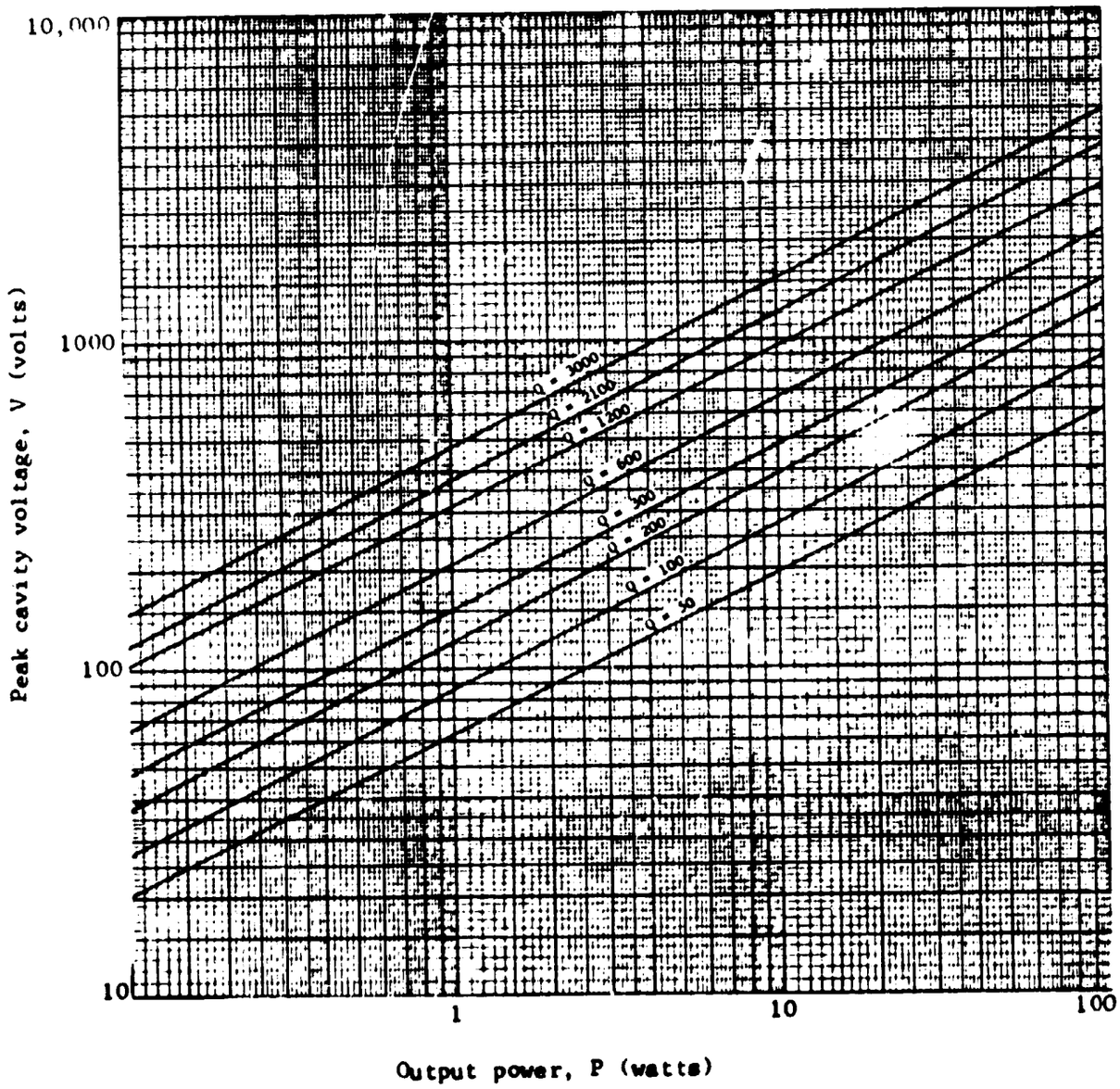

Figure 3-10. Peak cavity voltage versus output power for b/a = 2.72, where loaded Q is taken as a parameter.

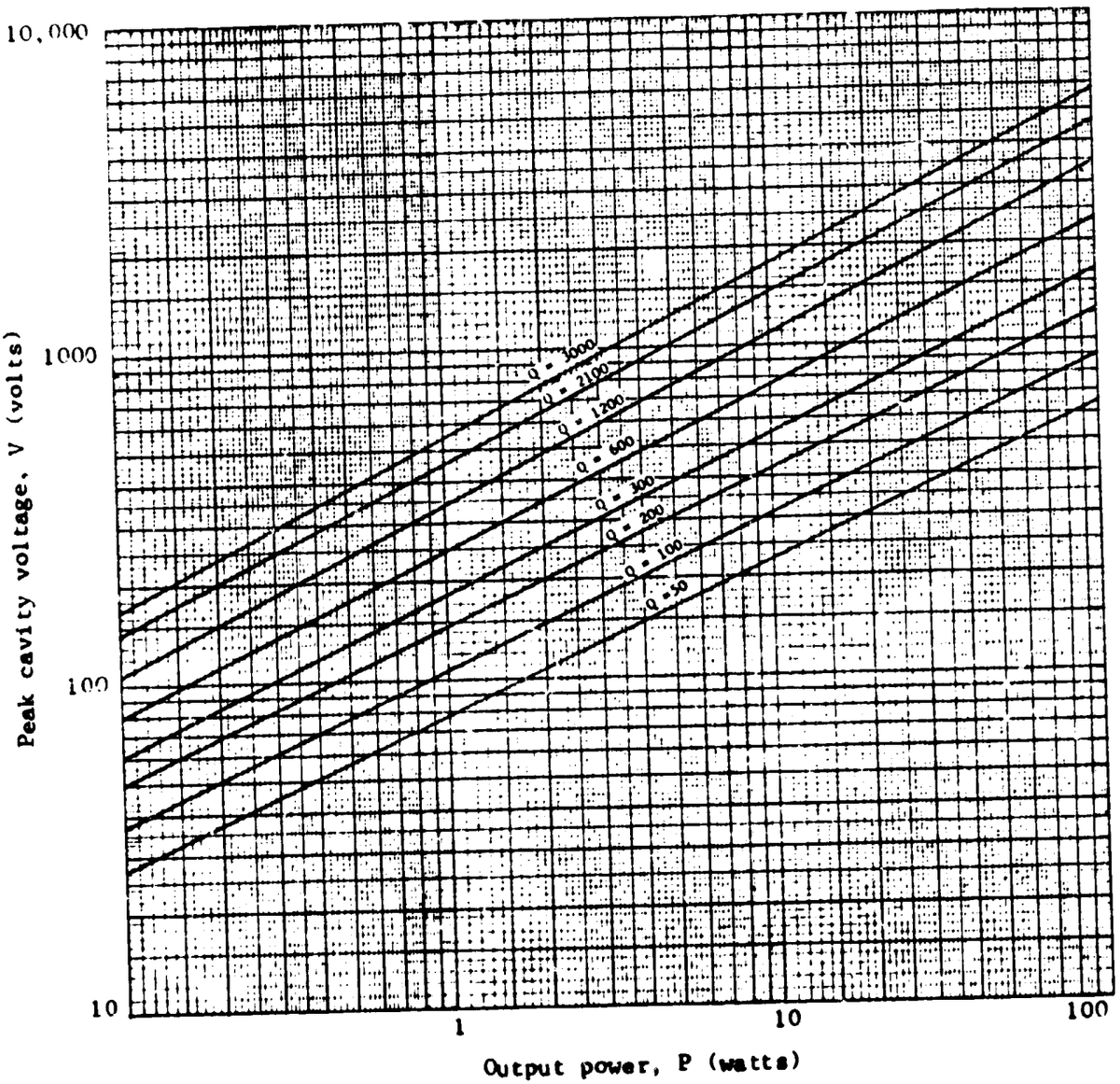

Figure 3-11. Peak cavity voltage versus output power for b/a = 3.6, where loaded Q is taken as a parameter.

4.0 FACTORS WHICH AFFECT STABILITY OF MULTICOUPLERS

Various complex electrical and mechanical factors enter into the stability of high Q multicoupler cavities. Specifically, there are two conditions of special interest in investigating stability: under normal ambient operating conditions and under breakdown conditions.

To facilitate analysis of cavity stability, the electrical equivalent circuit of a TEM mode coaxial cavity shown in figure 4-1 is adopted. For this model, the inductance is taken as that obtained by looking into a short circuited transmission line of characteristic impedance Z_o and length L less than a quarter wavelength long, namely

$$X_L = -jZ_o \tan kL \tag{4-1}$$

where $k = 2\pi/\lambda$. At resonance, the tuning capacitor value is computed on the basis of

$$jXc = -jX_L = Z_o \tan kL \tag{4-2}$$

from which

$$C = \frac{1}{\omega Z_o \tan kL} \tag{4-3}$$

For this model, the unloaded Q can be computed from the circuit relation

$$Q_o = \frac{1}{\omega_o CR} \tag{4-4}$$

where R is found on the basis of I^2R losses in the cavity walls. This was evaluated in Appendix A and given by the formula

$$Q_o = \frac{2b \ln (b/a)}{\delta (1 + b/a)} \quad . \tag{4-5}$$

In the following subsections, the problem of cavity stability based on this electrical model will be addressed.

4.1 Stability Under Ambient Conditions

The frequency stability of coaxial cavities under ambient conditions is closely dependent on temperature changes. From Appendix D, it is shown that differential thermal expansion of the center conductor is related to temperature change and the coefficient of linear expansion of the center conductor metal, α

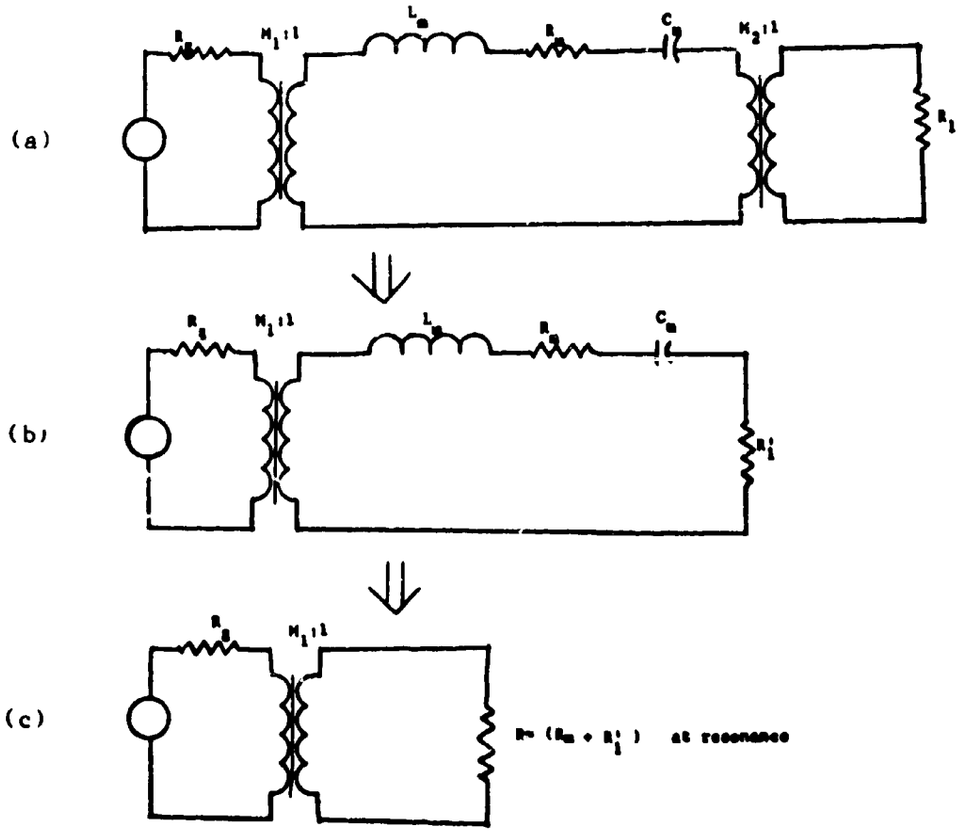

Figure 4-1 Equivalent circuit of a resonant cavity coupled to a generator and load. (The coupling mechanism is represented by means of ideal transformers.)

via

$$\Delta L = L \sigma \Delta T \quad . \tag{4-6}$$

This can be related to a change in resonant frequency of the cavity by assuming

$$L + \Delta L = L (1 + \sigma \Delta T) \approx \frac{\lambda}{4} \tag{4-7}$$

$$\frac{\lambda o}{4} (1 + \sigma \Delta T) = \frac{\lambda}{4} \tag{4-8}$$

from which

$$\frac{\lambda o}{\lambda} = \frac{f}{f_o} = \frac{1}{1 + \sigma \Delta T} \tag{4-9}$$

$$f = f_o (1 + \sigma \Delta T)^{-1} \quad ; \tag{4-10}$$

then

$$\frac{df}{dT} = -f_o (1 + \alpha \Delta T)^{-2} \sigma \tag{4-11}$$

where

$$\Delta T = (T - T_o) \quad .$$

Optimum stability of the microwave cavity is obtained via the following two steps:

A. Use materials to minimize the thermal expansion per equation (4-6): σ should be small.

B. Pick tuning capacitors with an inverse temperature drift coefficient as that given by equation (4-11) when evaluated under the maximum expected ΔT condition.

4.2 Stability Under Breakdown Conditions

In Appendix D the frequency shifts expected as the result of breakdown are investigated. For multipactor power levels which are typically in the order of 20 mw/cm^2 the frequency shift due to breakdown heating is less than 0.5 percent a negligible value.

What is probably more deleterious is the impedance effect of a breakdown on the electrical model of the cavity shown in figure 4-1. Since a corona or gas discharge is a very low impedance arc, the effect on the electrical model would be to series R_m with a very high value resistor, thus greatly mismatching the input along with a high internal loss due to the arc. As such, this must be interpreted as a total failure, and it is irrelevant to discuss stability for this breakdown mode.

On the other hand, a multipactor breakdown is not necessarily a total failure. If a cavity is viewed as a parallel LC resonant tank circuit, the effect of a multipactor is to parallel this model with an RC combination. The R will lower the loaded Q of the cavity and the C will detune the cavity. Depending on initial Q and tuning capacitor value, the effect might be tolerated without significant alteration to system operation.

5.0 RECOMMENDATION FOR DESIGN OF MULTICOUPLERS

In this section the results of this study are summarized. To review, the objective was to determine the design procedures necessary to suppress both multipactor breakdown in a space vacuum and gas breakdown at critical pressure. It was found that multipactor resonance can be adequately suppressed on the basis of judicious choice of a minimum f(b-a) product, while the requirements to suppress corona breakdown are far more stringent. Since at critical pressure, the corona threshold is only a function of electrical field strength, the only choice the designer has is to use low impedance and low Q circuits in order to minimize the electric field strength for a given power handling requirement. Even these approaches are limited and do not guarantee that the desired power handling requirement can be achieved.

In figure 5-1 a flow chart illustrates the procedures the designer must utilize in order to design multicouplers which are least susceptible to multipactor and corona breakdown. The application to a practical problem is illustrated in Appendix E.

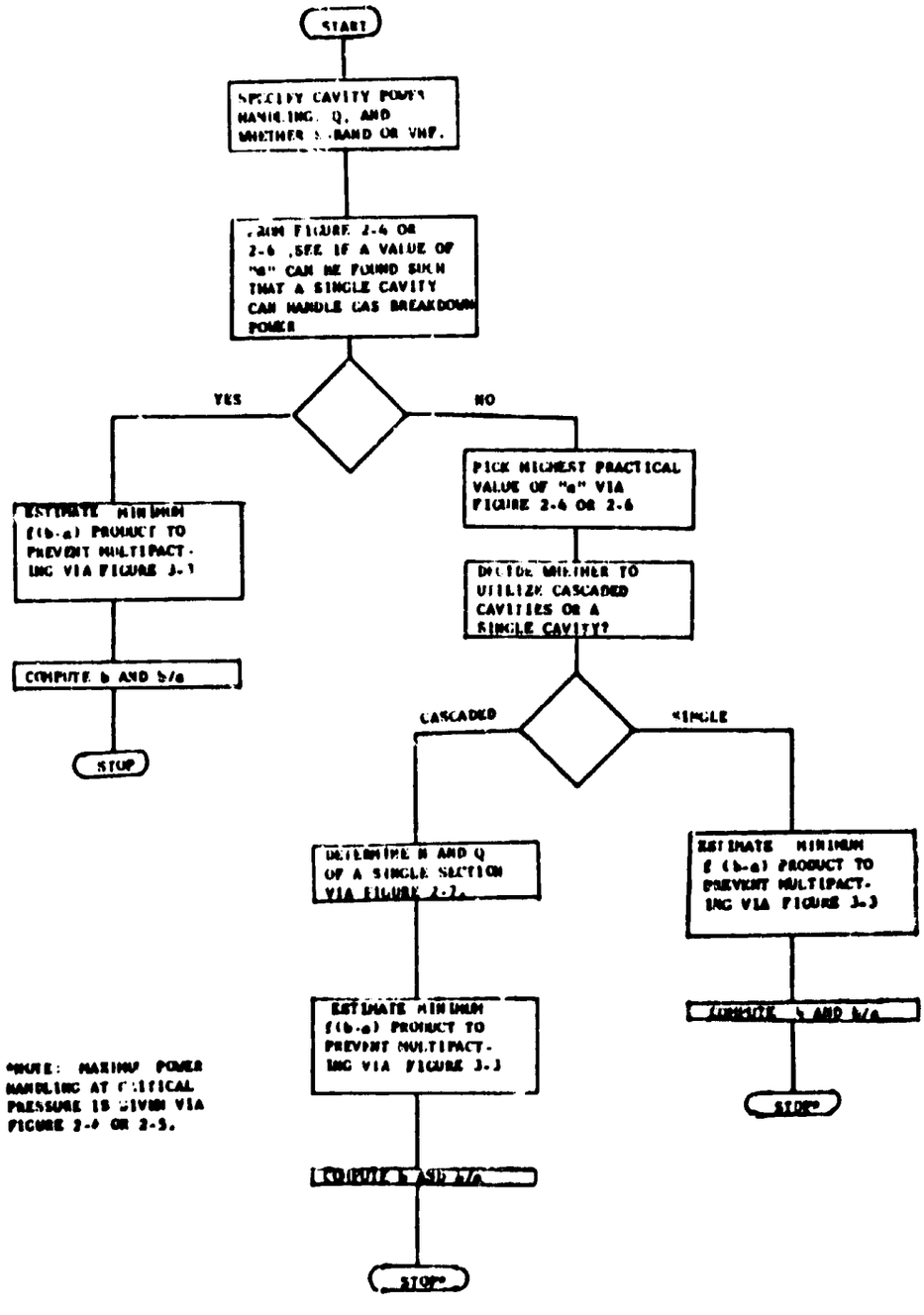

Figure 5-1. Flow chart illustrating design procedures to eliminate corona and multipactor breakdown in multicouplers.

6.0 REFERENCES

1. "Microwave Measurements", Edward Ginzton, McGraw-Hill Book Company, 1957.

2. "Measurements at Centimeter Wavelength", Donald D. King, D. Van Nostrand Company, Inc., 1952.

3. "Fields and Waves in Communication Electronics", Simon Ramo, John R. Whinnery, Theodore Van Duzer, John Wiley and Sons, Inc., 1965.

4. "Physics and Applications of Secondary Electron Emission", by Dr. H. Bruining, Pergamon Press, 1954.

5. "Mechanics of Material", Philip G. Laurson, William Junkin, John Wiley & Sons, Inc., 1954.

6. "Microwave Breakdown in Gases", A. D. MacDonald, John Wiley and Sons, Inc., 1966.

7. "Research on Microwave Window Mulcipactor and Its Inhibitions", Raymond Hayes, Final Report Eitel-McCullough, Inc., San Carlos, California, July 1964.

8. "Properties of Ionization Breakdown of Air at Microwave Frequencies and Optimization of Component Dimensions for Maximum Microwave Power", L. Rainwater, Sperry SSD Report Prepared for NASA Marshall Space Flight Center Under Contract NAS8-21812, Technical Directive 9-47, October 1971.

9. "Multipactor Breakdown in Space Electronics Systems", Dennis J. Kozakoff, Sperry Rand Corp. Technical Report SP-207-0428, December 1970.

10. "The Study of Multipactor Breakdown in Space Electronic Systems", NASA Report NASA CR-448, Goddard Space Flight Center, 1966. (Prepared by Hughes Aircraft under contract NAS5-3916).

11. "Experimental Results of Multipacting Between Coaxial Electrodes with High b/a Values", K. Woo, Supporting Research and Advanced Development for the Period October 1 to November 30, 1966, Space Programs Summary 37-42, Vol. IV, Jet Propulsion Laboratory, Pasadena, California, December 1966.

12. "Multipactor Discharge Experiments", E. F. Vance and J. E. Manevicz, Stanford Research Institute Scientific Report 5, ARCRL-68-0063, SRI Project 5359, Stanford Research Institute, Palo Alto, California, December 1967.

APPENDIX A

COMPUTATION OF MAXIMUM CAVITY VOLTAGE AS A FUNCTION OF POWER AND LOADED Q

The objective of this appendix is to derive relations for coaxial cavity electromagnetic fields that are not readily available in the technical literature.

MATHEMATICAL DEVELOPMENT

A solution to the problem of peak cavity voltage in terms of cavity parameters is posed based on an electromagnetic field theory type solution. The development begins with a restatement of Maxwell's equations, namely

(A-1) $$\nabla \times \bar{E} = -j\omega\mu\bar{H}$$

(A-2) $$\nabla \times \bar{H} = j\omega\epsilon\bar{E}$$

(A-3) $$\nabla \cdot \bar{B} = \nabla \cdot \bar{D} = 0$$

and the auxiliary relations

(A-4) $$B = \mu H$$

(A-5) $$D = \epsilon E \quad .$$

Only the condition for the dominant TEM mode is considered in this solution. With the a-priori knowledge that the only TEM field components existing in the principal coaxial mode are the E_r and H_ϕ field components, further assume that they are functions of the radius r. On this basis, the electromagnetic field inside a coaxial structure may be assumed to consist of wave propagation of the general form

(A-6) $$\bar{E} = E_r(r) \exp(-jkz)$$

and

(A-7) $$\bar{H} = H_\phi(r) \exp(-jkz) \quad .$$

With this assumption, it is readily shown that (A-1) reduces to

(A-8) $$\nabla \times \bar{E} = jk\bar{E}_r(r) \exp(-jkz) = -j\omega\mu\bar{H}_\phi(r) \exp(-jkz)$$

(A-9) $$E_r = \frac{\omega\mu}{k} H_\phi = \sqrt{\frac{\mu}{\epsilon}}\ \bar{H}_\phi$$

(A-10) $$E_r = \eta H_\phi$$

where η is the wave impedance, 120π ohms in free space. $\exp(jkz)$ propagation and $\exp(j\omega t)$ time variation is implicit in these equations.

Now assume that the peak electrical field magnitude can be taken as the gradient of a scalar potential field

(A-11) $$\bar{E} = -\nabla V$$

for which the Laplacian

(A-12) $$\nabla^2 V = 0 \quad .$$

Now to compute the form of V which will satisfy (A-12). This is especially simplified since V is assumed to be ϕ invariant. Solution to the Laplacian in cylindrical coordinates is as follows:

(A-13) $$\nabla^2 V = \frac{1}{r} \frac{\partial}{\partial r} \left(r \frac{\partial V}{\partial r}\right) = 0$$

(A-14) $$\left(r \frac{\partial V}{\partial r}\right) = C_1$$

(A-15) $$\frac{\partial V}{\partial r} = \frac{C_1}{r}$$

(A-16) $$V = C_1 \ln r + C_2$$

at r = a

(A-17) $$V = C_1 \ln a + C_2 = 0$$

at r = b

(A-18) $$V = C_1 \ln b + C_2 = V_o \quad .$$

The arbitrary coefficients of the differential equation can now be solved

(A-19) $$C_1 = \frac{\begin{bmatrix} 0 & 1 \\ V_o & 1 \end{bmatrix}}{\begin{bmatrix} \ln a & 1 \\ \ln b & 1 \end{bmatrix}} = \frac{V_o}{\ln(b/a)}$$

(A-20) $$C_2 = \frac{\begin{bmatrix} \ln a & 0 \\ \ln b & V_o \end{bmatrix}}{\begin{bmatrix} \ln a & 1 \\ \ln b & 1 \end{bmatrix}} = \frac{V_o \ln a}{\ln (b/a)}$$

from which

(A-21) $$V = \frac{V_o \ln (r/a)}{\ln (b/a)} \quad .$$

Now since E is the gradiant of V,

$$\bar{E}_r = -\frac{V_o}{r \ln(b/a)} \exp(-jkz) \qquad (A\text{-}22)$$

similarly, from (A-22) and (A-10),

$$\bar{H}_\phi = -\frac{V_o}{\eta r \ln(b/a)} \exp(-jkz) \qquad (A\text{-}23)$$

The problem for the coaxial resonator is now formulated by assuming the internal electromagnetic fields are composed of forward and reverse propagating waves. Therefore, on the basis of the right hand rule

$$\bar{E}_r = \bar{E}_r^{+} - \bar{E}_r^{-} \qquad (A\text{-}24)$$

$$= \frac{-V_o}{r \ln(b/a)} \exp(-jkz) + \frac{V_o}{r \ln(b/a)} \exp(+jkz)$$

$$\bar{E}_r = \frac{2jV}{r \ln(b/a)} \left[\frac{\exp(jkz) - \exp(-jkz)}{2j}\right] = \frac{j\,2V_o \sin kz}{r \ln(b/a)} \qquad (A\text{-}25)$$

and for the magnetic field component, H,

$$\bar{H}_\phi = \bar{H}_\phi^{+} + \bar{H}_\phi^{-} \qquad (A\text{-}26)$$

$$= \frac{-V_o}{r \ln(b/a)} \exp(-jkz) + \frac{-V_o}{r \ln(b/a)} \exp(+jkz)$$

$$\bar{H}_\phi = \frac{-2\,V_o}{\eta r \ln(b/a)} \left[\frac{\exp(jkz) + \exp(-jkz)}{2}\right] = \frac{-2\,V_o \cos kz}{\eta r \ln(b/a)} \qquad (A\text{-}27)$$

Taking $V = 2V_o$ = the maximum cavity voltage magnitude, the magnitudes of the electric and magnetic fields inside the cavity are taken to be

$$E_r = \frac{V \sin kz}{r \ln(b/a)} \qquad (A\text{-}28)$$

$$H_\phi = \frac{V \cos kz}{\eta r \ln(b/a)} \qquad (A\text{-}29)$$

From these, cavity Q can be computed. The total stored energy inside the cavity is evaluated via the volume integral

(A-30)
$$U = \iiint_{\text{volume}} \mu H^2 \, dv = \iiint_{\text{volume}} \epsilon E^2 \, dv \quad ;$$

then

(A-31)
$$U = \iiint_{\text{volume}} \epsilon \left[\frac{V \sin kz}{r \ln (b/a)}\right]^2 r \, dr d\phi \, dz$$

(A-32)
$$U = \frac{\epsilon V^2}{\ln^2 (b/a)} \iiint \frac{\sin^2 kz}{r} \, dr d\phi \, dz$$

(A-33)
$$U = \frac{\epsilon \pi L V^2}{\ln(b/a)} \quad .$$

The total power dissipated in the cavity is approximately that dissipated in the side walls and center conductor of the cavity, excluding the ends, and may be evaluated via the surface integral

(A-34)
$$Pd = \iint_{\text{center conductor}} \frac{1}{\sigma \delta} H_\phi^2 \, ds + \iint_{\text{outer wall}} \frac{1}{\sigma \delta} H_\phi^2 \, ds$$

(A-35)
$$Pd = \int_0^L \int_0^{2\pi} \frac{1}{\sigma \delta} \left[\frac{V \cos kz}{\eta b \ln(b/a)}\right]^2 b \, d\phi \, dz + \iint \frac{1}{\sigma \delta} \left[\frac{V \cos kz}{\eta a \ln(b/a)}\right]^2 a \, d\phi \, dz$$

(A-36)
$$Pd = \frac{\pi L V^2}{\eta^2 \delta \sigma \, b \ln^2(b/a)} + \frac{\pi L V^2}{\eta^2 \delta \sigma \, a \ln^2(b/a)}$$

(A-37)
$$Pd = \frac{\pi L V^2}{\eta^2 \sigma \delta \ln^2(b/a)} \left(\frac{1}{b} + \frac{1}{a}\right) = \frac{\pi L V^2 (1 + b/a)}{\eta^2 \, b \sigma \delta \ln^2(b/a)} \quad .$$

The basic definition for unloaded cavity Q, Q_o, is as follows:

(A-38)
$$Q_o = \frac{\omega W}{Pd}$$

where once again, U is the stored energy, and Pd is the average dissipated power inside the cavity. Then

(A-39) $$Q_o = \frac{\omega \epsilon \pi LV^2}{\ln(b/a)} \cdot \frac{\pi^2 b \sigma \delta \ln^2(b/a)}{\pi LV^2 (1 + b/a)}$$

$$= \frac{\omega \epsilon \sigma \delta b \pi^2 \ln(b/a)}{(1 + b/a)} = \frac{\omega \mu \sigma \delta b \ln (b/a)}{(1 + b/a)}$$

but

(A-40) $$\delta = \sqrt{\frac{1}{\pi f \mu \sigma}} \quad ;$$

therefore,

(A-41) $$Q_o = 2\pi f \mu \sigma \sqrt{\frac{1}{\pi f \mu \sigma}} \cdot \frac{b \ln(b/a)}{(1 + b/a)}$$

$$= \sqrt{\pi f \mu \sigma} \cdot \frac{2b \ln(b/a)}{(1 + b/a)}$$

(A-42) $$Q_o = \frac{2b \ln(b/a)}{\delta (1 + b/a)} \quad .$$

This agrees exactly with equation (7.21) in Ginzton [1].

The problem of loaded Q is attacked by noting the external Q is related to output power via

(A-43) $$Q_{ext} = \frac{\omega U}{P_o} \quad ;$$

we also note the relation

(A-44) $$\frac{1}{Q_L} = \frac{1}{Q_{ext}} + \frac{1}{Q_o}$$

from which

(A-45) $$Q_L = Q_{ext} \left(1 - \frac{Q_L}{Q_o}\right) = \frac{\omega U}{P_o} \left(1 - \frac{Q_L}{Q_o}\right) \quad .$$

Incorporating equation (A-33)

$$Q_L = \frac{\omega \epsilon \pi L V^2}{P_o \ln(b/a)} \left(1 - \frac{Q_L}{Q_o}\right) \quad . \tag{A-46}$$

For a quarter wavelength cavity, equation (A-46) can be solved with the following result

$$V = \sqrt{\frac{2P_o \eta \ Q_L \ln(b/a)}{\pi^2 \left(1 - \frac{Q_L}{Q_o}\right)}} \quad . \tag{A-47}$$

For a small loaded to unloaded Q ratio, the term Q_L/Q_o in the denominator can be ignored.

Since the characteristic impedance for a coaxial line is given by the relation

$$Z_o = \frac{60}{\sqrt{\epsilon_r}} \ln(b/a) \quad , \tag{A-48}$$

then equation (A-47) may also be expressed via

$$V = \sqrt{\frac{4 P_o Q_L Z_o}{\pi \left(1 - \frac{Q_L}{Q_o}\right)}} \tag{A-49}$$

from which is shown that peak cavity voltage is proportional to both Q and Z_o.

The results of this derivation are plotted in figures 3-9, 3-10, and 3-11, of the main text of this report.

APPENDIX B

COMPUTATION OF MAXIMUM CAVITY VOLTAGES AS A FUNCTION OF POWER LEVEL AND LOADED Q, NON-TEM MODES

The objective of this appendix is to investigate higher order modes which may exist in coaxial resonators, and subsequently, derive electromagnetic field relations in terms of power level and Q. This mathematical development is not currently available in the technical literature.

MATHEMATICAL DEVELOPMENT

The desired solution is obtained via rigorous solutions of the field equations. Starting with Maxwell,

(B-1) $$\nabla.\bar{B} = \nabla.\bar{D} = 0 \quad ,$$

(B-2) $$\nabla \times \bar{E} = -j\omega\mu\bar{H} \quad ,$$

and

(B-3) $$\nabla \times \bar{H} = j\omega\epsilon\bar{E} \quad ;$$

then

(B-4) $$\nabla \times \nabla \times \bar{E} = -j\omega\mu\nabla \times \bar{H} = -j\omega\mu\,(j\omega\epsilon\bar{E})$$
$$= \omega^2\mu\epsilon\bar{E} = k^2\bar{E} \quad .$$

By vector relation:

(B-5) $$\nabla \times \nabla \times \bar{E} = \nabla(\nabla.\bar{E}) - \nabla^2\bar{E} \quad ,$$

we get

(B-6) $$\nabla^2\bar{E} = -k^2\bar{E} \quad ;$$

similarly

(B-7) $$\nabla^2\bar{H} = -k^2\bar{H} \quad .$$

Now for non-TEM modes in coaxial line, it is recognized that the three-dimensional ∇^2 may be broken up into two parts,

(B-8) $$\nabla^2 = \nabla_t^2 + \frac{\partial^2}{\partial z^2} \quad .$$

By assuming propagation as $e^{-\gamma Z}$ in the Z-direction

(B-9) $$\frac{\partial^2}{\partial Z^2} = \gamma^2 \quad .$$

Hence, for electric field components

(B-10) $$\nabla^2 \bar{E} = \nabla_t^2 \bar{E} + \gamma^2 \bar{E} = -k^2 \bar{E}$$

from which

(B-11) $$\nabla_t^2 \bar{E} = -(\gamma^2 + k^2) \bar{H} = -k_c^2 \bar{E} \quad ;$$

similarly,

(B-12) $$\nabla_t^2 \bar{H} = -(\gamma^2 + k^2) \bar{H} = -k_c^2 \bar{H}$$

from which

(B-13) $$k_c^2 = (\gamma^2 + k^2) = \gamma^2 + \omega^2 \mu \epsilon \quad ,$$

(B-14) $$\gamma^2 = k_c^2 - k^2 = k_c^2 - \omega^2 \mu \epsilon \quad ,$$

(B-15) $$\gamma = \sqrt{k_c^2 - \omega^2 \mu \epsilon} \quad .$$

Above cutoff, γ must be an imaginary number.

The coaxial line problem can now be addressed by noting that the two-dimensional ∇_t^2 may be written in terms of cylindrical coordinates.

For TM waves $H_Z = 0$ and

(B-16) $$\nabla_t^2 E_Z = \frac{\partial^2 E_Z}{\partial r^2} + \frac{1}{r} \frac{\partial E_Z}{\partial r} + \frac{1}{r^2} \frac{\partial^2 E_Z}{\partial \phi^2} = -k_c^2 E_Z \quad .$$

For TE waves $E_Z = 0$ and

(B-17) $$\nabla_t^2 H_Z = \frac{\partial^2 H_Z}{\partial r^2} + \frac{1}{r} \frac{\partial H_Z}{\partial r} + \frac{1}{r^2} \frac{\partial H_Z}{\partial \phi^2} = -k_c^2 H_Z \quad .$$

In order to obtain two ordinary differential equations, solve for the transverse field components by assuming a product solution and separate variables.

Assume a product solution of the following forms:

for TM modes $H_Z = 0$ and

(B-18) $$E_Z = R \cdot F_\phi \quad ,$$

for TE modes $E_Z = 0$ and

(B-19) $$H_Z = R \cdot F_\phi \quad ,$$

where R is a function of r only, and F_ϕ a function of ϕ only.

On this basis (B-16) or (B-17) becomes

(B-20) $$R'' F_\phi + R' \frac{F_\phi}{r} + \frac{F_\phi'' R}{r^2} = -k_c^2 R F_\phi$$

(B-21) $$r^2 \frac{R''}{R} + r \frac{R'}{R} + k_c^2 r^2 = -\frac{F_\phi''}{F_\phi} = \gamma^2 \quad .$$

From (B-21) the two separated differential equations to be solved are

(B-22) $$F_\phi'' = -\gamma^2 F_\phi$$

(B-23) $$R'' + \frac{1}{r} R' + \left(k_c^2 - \frac{\gamma^2}{r}\right) R = 0 \quad .$$

By basic calculus, the solutions to (B-22) and (B-23) take the following forms, respectively

(B-24) $$F_\phi = A \cos \gamma \phi + B \sin \gamma \phi$$

(B-25) $$R = C J_\gamma (k_c r) + D N_\gamma (k_c r)$$

where A, B, C and D are arbitrary constants.

Now establish that all other field components are obtainable in terms of the z-directed components by the following relations:

(B-26) $$E_r = -\frac{1}{k_c^2} \left[\gamma \frac{\partial E_Z}{\partial r} + \frac{j\omega\mu}{r} \frac{\partial H_Z}{\partial \phi}\right] \quad ,$$

C.2

(B-27) $$E_\phi = \frac{1}{k_c^2}\left[-\frac{\gamma}{r}\frac{\partial E_Z}{\partial \phi} + j\omega\mu\frac{\partial H_Z}{\partial r}\right] ,$$

(B-28) $$H_r = \frac{1}{k_c^2}\left[\frac{j\omega\epsilon}{r}\frac{\partial E_Z}{\partial \phi} - \gamma\frac{\partial H_Z}{\partial R}\right] ,$$

(B-29) $$H_\phi = -\frac{1}{k_c^2}\left[j\omega\epsilon\frac{\partial E_Z}{\partial r} + \frac{\gamma}{r}\frac{\partial H_Z}{\partial \phi}\right] .$$

TM and TE waves are now treated separately.

TM WAVES IN COAXIAL LINES

It is desired to derive expressions and cutoff relations for the $TM_{\gamma p}$ modes in (B-24) and B-25), where p pertains to the p th root of the Bessel and Neumann functions.

For TM waves, boundary conditions require E_Z be zero at r = a and b, respectively. Hence

(B-30) $$A_\gamma J_\gamma (k_c a) + B_\gamma N_\gamma (k_c a) = 0 ,$$

(B-31) $$A_\gamma J_\gamma (k_c b) + B_\gamma N\gamma (k_c b) = 0 ,$$

and the cutoff condition

(B-32) $$\frac{N_\gamma (k_c a)}{J_\gamma (k_c a)} = \frac{N_\gamma (k_c b)}{J_\gamma (k_c b)} .$$

Solution to this transcendental equation can be done graphically. Specifically, for b/a = 3.5 (case of highest Q), Ramo-Whinnery-Van Duzer [3] give the following solutions for the first p=1 roots.

(B-33) TM_{01} $\lambda_c \approx 2.2\ (b-a)$,

(B-34) TM_{11} $\lambda_c \approx 1.76\ (b-a)$,

(B-35) TM_{21} $\lambda_c \approx 1.60\ (b-a)$,

etc.

TE WAVES IN COAXIAL LINES

In this subsection it is desired to investigate cutoff relations for the $TE_{\gamma p}$ modes.

Since the boundary conditions for TE modes require the derivative of H_Z be zero at the surfaces, then by differentiating (B-30) and (B-31), the cutoff condition is obtained.

(B-36) $$\frac{N'_\gamma (k_c a)}{J'_\gamma (k_c a)} = \frac{N'_\gamma (k_c b)}{J'_\gamma (k_c b)}$$

For the p=1 roots, the cutoff wavelength for all other $TE_{\gamma 1}$ roots are

(B-37) $$\lambda_c \approx \frac{2\pi}{\gamma} \left(\frac{b+a}{2}\right) \; ; \; \gamma = 1,2,3 \ldots \quad .$$

Thus the lowest order TE modes are

(B-38) $$TE_{11} \quad \lambda_c \approx 2\pi \left(\frac{b+a}{2}\right) = \pi (b+a) \; ,$$

(B-39) $$TE_{21} \quad \lambda_c \approx \pi \left(\frac{b+a}{2}\right) = \frac{\pi}{2} (b+a) \; ,$$

(B-40) $$TE_{31} \quad \lambda_c \approx \frac{2\pi}{3} \left(\frac{b+a}{2}\right) = \frac{\pi}{3} (b+a) \; ,$$

etc.

Now, investigate mode cutoffs for typical b/a ratios. Specifically, for the b/a ratio corresponding to highest Q (3.5), for the TM_{01} mode from (B-33)

(B-41) $$\lambda_c = 2.2(b-a) = 2.2 \; (3.5a-a) = 5.5a \quad ,$$

from (B-38) for the TE_{11} mode

(B-42) $$\lambda_c = \pi(b+a) = \pi(3.5a+a) = 4.5\pi a = 14.2a \quad .$$

It can be concluded from (B-41) and (B-42) that the TE_{11} mode will be the first higher order mode to occur and this mode will be treated in the balance of this analysis.

SOLUTION FOR H_{11} ELECTROMAGNETIC FIELD COMPONENTS

From (B-26) through (B-29) for $E_Z = 0$

$$E_r = -\frac{j\omega\mu}{k_c^2 r}\frac{\partial H_Z}{\partial \phi} \quad , \tag{B-43}$$

$$E_\phi = \frac{j\omega\mu}{k_c^2}\frac{\partial H_Z}{\partial r} \quad , \tag{B-44}$$

$$H_r = \frac{\gamma}{k_c^2}\frac{\partial H_Z}{\partial r} \quad , \tag{B-45}$$

$$H_\phi = \frac{-\gamma}{k_c^2 r}\frac{\partial H_Z}{\partial \phi} \quad . \tag{B-46}$$

The internal cavity fields are taken as the sum of forward and reverse going waves.

$$H_Z = H_Z^+ + H_Z^- \tag{B-47}$$

$$H_Z = 2 \cos \gamma Z \cos \phi \left[CJ_1(k_c r) + DN_1(k_c r) \right] . \tag{B-48}$$

Boundary conditions required

$$CJ_1'(k_c a) + DN_1'(k_c a) = 0 \tag{B-49}$$

$$C = \frac{-N_1'(k_c a)}{J_1'(k_c a)} D \quad . \tag{B-50}$$

Hence,

$$H_Z = 2 \cos \gamma Z \cos \phi \left[J_1 C(k_c r) - \left[\frac{J_1'(k_c a)}{N_1'(k_c a)}\right] CN_1(k_c r) \right] \quad ; \tag{B-51}$$

let $H_o = C \times 2$

(B-52) $$H_Z = H_o \cos \gamma Z \cos \phi \left[J_1(k_c r) - \left[\frac{J_1'(k_c a)}{N_1'(k_c a)}\right] N_1(k_c r)\right] ,$$

from (B-43)

(B-53) $$E_r = \frac{+j\omega\mu}{k_c^2 r} H_o \sin \gamma Z \sin \phi \left[J_1(k_c r) - \left[\frac{J_1'(k_c a)}{N_1'(k_c a)}\right] N_1(k_c r)\right] ,$$

from (B-44)

(B-54) $$E_\phi = \frac{j\omega\mu}{k_c} H_o \sin \gamma Z \cos \phi \left[J_1'(k_c r) - \left[\frac{J_1'(k_c a)}{N_1'(k_c a)}\right] N_1'(k_c r)\right] ,$$

from (B-45)

(B-55) $$H_r = \frac{\gamma}{k_c} H_o \cos \gamma Z \cos \phi \left[J_1'(k_c r) - \left[\frac{J_1'(k_c a)}{N_1'(k_c a)}\right] N_1'(k_c r)\right] ,$$

and from (B-46)

(B-56) $$H_\phi = \frac{\gamma}{k_c^2 r} H_o \cos \gamma Z \sin \phi \left[J_1(k_c r) - \left[\frac{J_1'(k_c a)}{N_1'(k_c a)}\right] N_1(k_c r)\right] .$$

COMPUTATION OF ARBITRARY CONSTANTS

Since by definition of loaded cavity Q

(B-57) $$Q = \frac{\omega U}{P_o}$$

(B-58) $$U = \frac{Q P_o}{\omega} = \text{stored energy/cycle} .$$

Now recognizing the fact that the total stored energy/cycle in the electric and magnetic fields must be the same, then

(B-59) $$U = \int_{\text{volume}} \epsilon E^2 \, dv ,$$

(B-60)
$$U = \int_0^L \int_a^b \int_0^{2\pi} \frac{\epsilon\omega^2\mu^2}{k_c^4 r^2} H_o^2 \sin^2 \gamma z \sin^2 \phi \left[J_1(k_c r) - \left[\frac{J_1'(k_c a)}{N_1'(k_c a)} \right] N_1(k_c r) \right]$$

$$\cdot\, r\,d\theta\,dr\,dz$$

$$+ \int_0^L \int_a^b \int_0^{2\pi} \frac{\epsilon\omega^2\mu^2}{k_c^2} H_o^2 \sin^2 \gamma z \cos^2 \phi \left[J_1'(k_c r) - \left[\frac{J_1'(k_c a)}{N_1'(k_c a)} \right] N_1'(k_c r) \right]^2 - r\,d\theta\,dr\,dz$$

(B-61)
$$U = \frac{\epsilon\omega^2\mu^2 H_o^2 \pi L}{k_c^4 \cdot 2} \int_a^b \frac{1}{r^2} \left[J_1(k_c r) - \left[\frac{J_1'(k_c a)}{N_1'(k_c a)} \right] N_1(k_c r) \right]^2 dr$$

$$+ \frac{\epsilon\omega^2\mu^2 H_o^2 \pi L}{k_c^2 \; 2} \int_a^b r \left[J_1'(k_c r) - \left[\frac{J_1'(k_c a)}{N_1'(k_c a)} \right] N_1'(k_c r) \right]^2 dr \quad .$$

Recognizing that the second integral contributes most of the energy, let

$$A = \frac{\epsilon\omega^2\mu^2 H_o^2 \pi L}{2k_c^2} = \frac{\epsilon\omega^2\mu^2 H_o^2 \pi\lambda}{8k_c^2} = \frac{\epsilon\omega\mu^2 H_o^2 \pi^2 c}{4k_c^2}$$

$$= \sqrt{\mu\epsilon}\sqrt{\mu\epsilon}\,\frac{\omega\mu H_o^2 \pi^2 c}{4k_c^2} = \frac{\omega\mu H_o^2 \pi^2}{4\,C\,k_c^2} \quad ,$$

$$B = \frac{-J_1'(k_c a)}{N_1'(k_c a)} = \frac{-J_1'(k_c b)}{N_1'(k_c b)} \quad ;$$

then

(B-62)
$$U \approx A \int_a^b r \left[J_1'(k_c r) + B N_1'(k_c r) \right]^2 dr \quad ,$$

(B-63) $$U \approx A \int_a^b r \left[J_1'(k_c r)\right]^2 + B^2 r \left[N_1'(k_c r)\right]^2 dr$$

$$= A \int_a^b r \left[J_o(k_c r) - \frac{1}{k_c r} J_1(k_c r)\right]^2 dr$$

$$+ AB^2 \int_a^b r \left[N_o(k_c r) - \frac{1}{k_c r} N_1(k_c r)\right]^2 dr \quad ,$$

(B-64) $$U \leq A \int_a^b r J_o^2(k_c r)\, dr + AB^2 \int_a^b r N_o^2(k_c r)\, dr \quad .$$

Now since

$$\int r R_r^2(k_c r) dr = \frac{r^2}{2} \left[R_\gamma^2(k_c r) - R_{\gamma-1}(k_c r) R_{\gamma+1}(k_c r)\right]$$

and $$J_{-1}(k_c r) = -J_1(k_c r) \quad ,$$

(B-65) $$U \leq A \left\{ \frac{b^2}{2} \left[J_o^2(k_c b) + J_1^2(k_c b)\right] - \frac{a^2}{2} \left[J_o^2(k_c a) + J_1^2(k_c a)\right] \right\}$$

$$+ AB^2 \left\{ \frac{b^2}{2} \left[N_o^2(k_c b) + N_1^2(k_c b)\right] - \frac{a^2}{2} \left[N_o^2(k_c a) + N_1^2(k_c a)\right] \right\} .$$

Taking the identity, and equation (B-58)

(B-66) $$\frac{QP_o}{\omega} = \frac{\omega\mu H_o^2 \pi^2}{8c K_c^2} \left\{ b^2 J_o^2(k_c b) + B^2 J_1^2(k_c b) - a^2 J_o^2(k_c a) - a^2 J_1^2(k_c a) \right\}$$

$$+ \frac{\omega\mu H_o^2 \pi^2}{8c k_c^2} B^2 \left\{ b^2 N_o^2(k_c b) + b^2 N_1^2(k_c b) - a^2 N_o^2(k_c a) - a^2 N_1^2(k_c a) \right\}$$

$$H_o^2 = \frac{8\pi k_c^2}{\omega\mu\pi^2} \cdot \frac{QP_o}{\omega}$$

$$\left\{ b^2 J_o^2 (k_c b) + b^2 J_1^2 (k_c b) - a^2 J_o^2 (k_c a) - a^2 J_1^2 (k_c a) \right.$$

$$\left. + B^2 b^2 N_o^2 (k_c b) + B^2 b^2 N_1 (k_c b) - B^2 a^2 N_o^2 (k_c a) - B^2 a^2 N_1^2 (k_c a) \right\} . \quad \text{(B-67)}$$

In conclusion

$$H_o^2 = \frac{8\pi k_c^2 QP}{K_1 \omega^2 \mu\pi^2} = \frac{8\omega_c^2 QP}{K_1 \omega^2 \mu\pi^2 c} = \left(\frac{\omega_c}{\omega}\right)^2 \frac{8QP}{K_1 \mu\pi^2 c} = \left(\frac{\omega_c}{\omega}\right)^2 \frac{8QP}{K_1 \pi^2 \eta} \quad \text{(B-68)}$$

where

$$K_1 = \left\{ b^2 \left[J_o^2 (k_c a) + J_1^2 (k_c b) \right] - a^2 \left[J_o^2 (k_c a) + J_1^2 (k_c a) \right] \right.$$

$$+ \left[\frac{J_1' (k_c a)}{N_1' (k_c a)} \right] b^2 \left[N_o^2 (k_c b) + N_1^2 (k_c b) \right]$$

$$\left. - \left[\frac{J_1' (k_c a)}{N_1' (k_c a)} \right] a^2 \left[N_o^2 (k_c a) + N_1^2 (k_c a) \right] \right\} . \quad \text{(B-69)}$$

APPENDIX C

ANALYSIS OF MINIMUM fd PRODUCT TO PREVENT MULTIPACTING FOR TEM MODE COAXIAL CAVITIES

In this appendix the results of Appendix A are used together with the lower bound on multipacting voltage (equation 3-1) derived within the text, to compute minimum fd product to insure no multipacting for a given power level and cavity loaded Q.

For a given peak cavity voltage, the minimum fd product below which multipaction is supported is

$$fd = 0.894\, V^{1.176} \quad . \tag{C-1}$$

The derived expression for peak cavity voltage in terms of cavity parameters is given via

$$V = \left\{ \frac{2\eta Q P \ln (b/a)}{\pi^2} \right\}^{1/2} . \tag{C-2}$$

Hence,

$$fd = 0.894 \left\{ \frac{2\eta Q P \ln (b/a)}{\pi^2} \right\}^{\frac{1.176}{2}} . \tag{C-3}$$

The following Fortran computer program was written and executed to compute numerical values:

```
// FOR
*LIST SOURCE PROGRAM
*IOCS(CARD,1132 PRINTER,DISK)
    25 READ(2,50)X
    50 FORMAT(10X,F10.3)
       IF(X-0) 500,500,60
    60 CONTINUE
C      PROGRAM TO COMPUTE MAXIMUM CAVITY VOLTAGE
C      AS FUNCTION OF LOADED Q AND POWER
       PI=3.14159265
       ETA=120.*PI
       C=PI**2
       DO 200 I=1,10
       QL=300.*I
       WRITE (3,250)
   250 FORMAT(1H1,50HCOMPUTATION OF COAXIAL CAVITY VOLTAGE VERSUS POWER//)
       WRITE(3,300)X,QL
   300 FORMAT(1HI,10HB/A RATIO=,F6.2,10X,16HLOADED CAVITY Q=,F10.0//)
       WRITE(3,301)
   301 FORMAT(1H ,10X,14HPOWER IN WATTS,10X,19HPEAK CAVITY VOLTAGE,
      110X,20HMINIMUM FD IN MHZ-CM//)
       DO 350 J=1,100
       P=0.1*J
       A=2.*QL*P*ETA*ALOG(X)
       V=SQRT(A/C)
       FD=0.894*(V**1.176)
       WRITE(3,400)P,V,FD
   400 FORMAT(14X,F6.2,18X,F12.2,18X,F10.2)
   350 CONTINUE
   200 CONTINUE
       GO TO 25
   500 CONTINUE
       STOP
       END

FEATURES SUPPORTED
 IOCS

CORE REQUIREMENTS FOR
 COMMON       0  VARIABLES      24  PROGRAM     290

END OF COMPILATION

// XEQ
```

The numerical results of the program execution are plotted in figures 3-2 through 3-4 in the main text of this report.

APPENDIX D

INSTABILITY OF COAXIAL CAVITIES DUE TO BREAKDOWN HEATING

The purpose of this appendix is to investigate the stability of coaxial cavities as related to multipactor or gas breakdowns. In the approach taken, the mechanical thermal expansion of the center conductor element is computed for two different types of breakdowns in order to verify whether or not the mechanical geometrical changes due to heating are significant; that is, breakdown between center conductor and top wall, and breakdown between center conductor and sidewalls.

Case 1. Breakdown between top of the coaxial center conductor and the top of the coaxial cavity, as illustrated in figure D-1.

For this case assume the entire heat load is conducted into the top of the center conductor element. From thermodynamic relations, the applicable differential equation is

$$\frac{dT}{dx} = \frac{q}{kA} = \frac{q}{k(\pi a^2)} \tag{D-1}$$

where k is the coefficient of thermal conductivity, q is the heat input in BTU/hr, and (πa^2) is the center conductor cross sectional area in ft^2. By integrating (D-1),

$$T = \frac{qx}{k(\pi a^2)} + C_1 \tag{D-2}$$

from boundary conditions; at x=0, $T=T_a$, therefore $C_1 = T_a$ and

$$T = \frac{qx}{k(\pi a^2)} + T_A \tag{D-3}$$

Now, the differential thermal expansion of a linear element is related to temperature change and the coefficient of linear expansion, α, via

$$\Delta L = L \alpha \Delta T \tag{D-4}$$

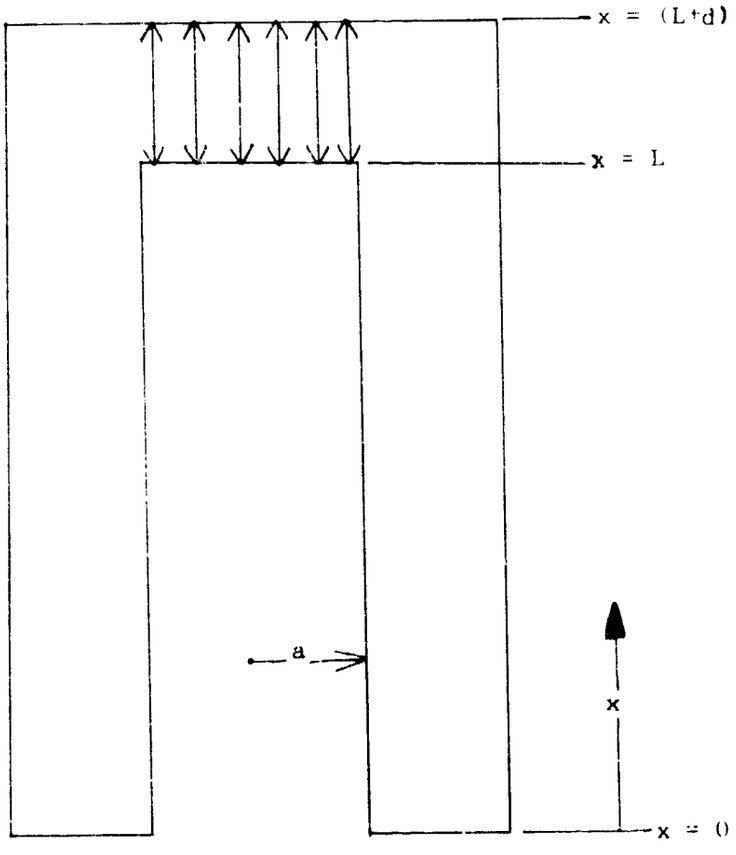

Figure D-1. Breakdown between center conductor and top wall of coaxial cavity.

where ΔT is in ^{o}F, L and ΔL are in units of feet. From this relation and (D-3) a worst case expansion can be evaluated on the basis of

(D-5) $$\Delta L = L\,\alpha(T-T_A) = \frac{\alpha q L^2}{k(\pi a^2)} \quad .$$

This length change can be related to a change in the resonant frequency of the cavity by assuming the center conductor to be a quarter wavelength at the resonant wavelength. Then

(D-6) $$L + \frac{\alpha q L^2}{k(\pi a^2)} = \frac{\lambda}{4} \quad ,$$

(D-7) $$\frac{\lambda o}{4} + \frac{\alpha q \lambda_o^2}{16\, k(\pi a^2)} = \frac{\lambda}{4} \quad ,$$

from which the result is

(D-8) $$\frac{\lambda o}{\lambda} = \frac{f}{f_o} = \frac{1}{\left\{1 + \left[\frac{\alpha q \lambda_o}{4\, k(\pi a^2)}\right]\right\}} \quad .$$

It is now an academic interest to specifically evaluate (D-8) for certain special conditions. Assume the cavity material to be aluminum, the following constants are obtained from the material handbooks:

$$\alpha\ (ft/ft/^{o}F) = 0.000013 = 13\times10^{-6}$$

$$k\ (BTU/hr\text{-}ft\text{-}^{o}F) = 140 \quad .$$

Equation (D-8) is then expressed

(D-9) $$\frac{f}{fo} = \frac{1}{\left[1 + 2.32\times10^{-8}\ \frac{q\lambda o}{\pi a^2}\right]} \quad .$$

At this point in the development, it is convenient to characterize a breakdown in terms of breakdown power density P ($watts/cm^2$). Since the heat input, q, is related to watts via

(D-10) $$q(BTU/hr) = 3.413\ q(watts) \quad ,$$

then, in terms of the power density P,

(D-11) $$q(\text{BTU/hr}) = 3.413\, q(\text{watts}) = 3.413PA = 3.413P\,(\pi a^2) \quad .$$

From (D-10) and (D-11),

(D-12) $$\frac{f}{f_o} = \frac{1}{\left[1 + 2.42\times10^{-6}\, P\lambda_o\right]} \quad .$$

Considering a VHF cavity (250 MHz), a wavelength is approximately 122 centimeters in which case

(D-13) $$\frac{f}{f_o} = \frac{1}{1 + 3.10\times10^{-4}\, P} \quad .$$

This result is plotted in figure D-2.

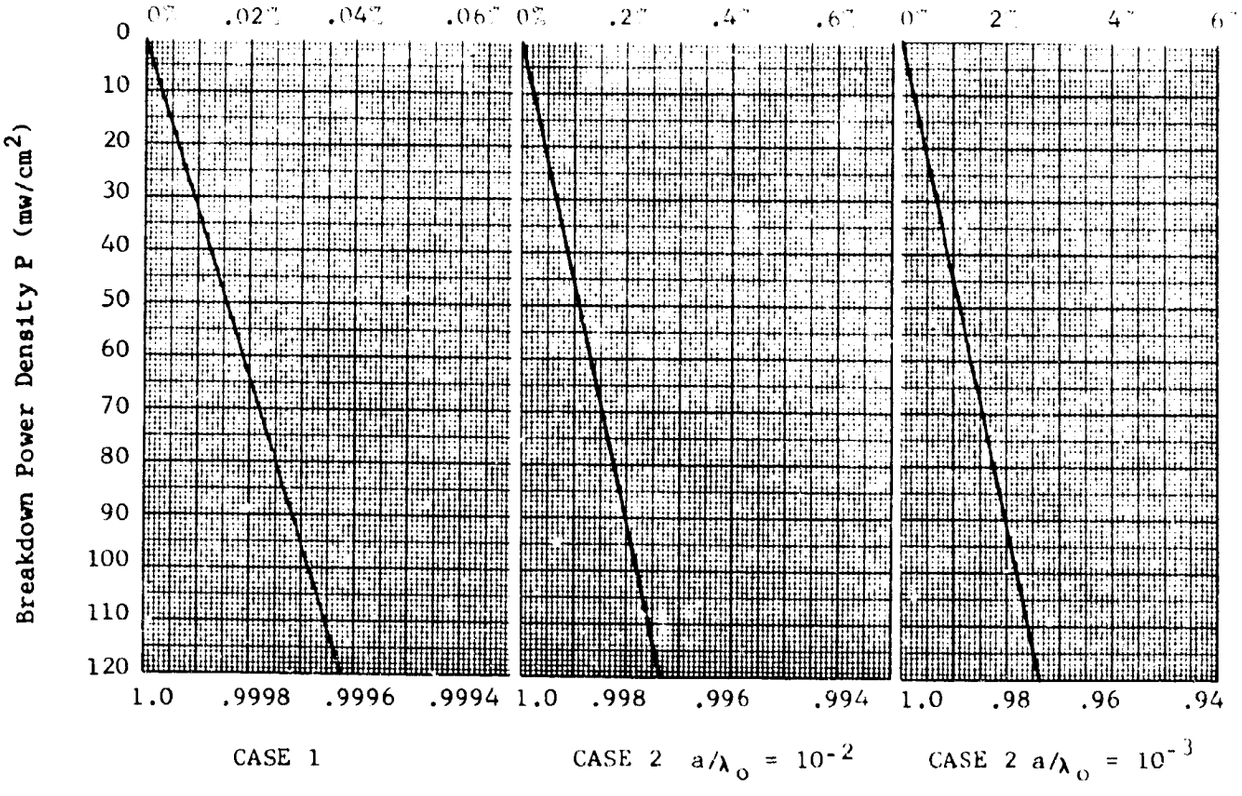
Percentage Frequency Change
0% .02% .04% .06% 0% .2% .4% .6% 0% 2% 4% 6%
Breakdown Power Density P (mw/cm²)
0
10
20
30
40
50
60
70
80
90
100
110
120
1.0 .9998 .9996 .9994
1.0 .998 .996 .994
1.0 .98 .96 .94
CASE 1
CASE 2 a/λo = 10⁻²
CASE 2 a/λo = 10⁻³
f/fo

Figure D-2

Case 2. Breakdown between center conductor and the sidewalls.

From the multipacting and gas breakdown equations, it is noted that for a fixed fd product, multipacting breakdown can occur over a range of voltage. Since the voltage distribution along the center conductor varies in approximately a sinusoidal fashion, there will be a range of center conductor area over which breakdown will occur, as illustrated in figure D-3. To simplify the analysis, once again assume that the breakdown can be characterized by a breakdown power density P watts/cm^2) over the breakdown region of the center conductor, resultant heating of the center conductor with thermal expansion and a corresponding shift in frequency.

This condition is more difficult than case 1, and it is necessary to treat the problem in terms of two independent solutions: solution in the breakdown region (region 1) where uniform heating over the center conductor exists, and a solution in region 2, where the breakdown heating power is conducted away.

From thermodynamic relations, the applicable differential equation in region 1 is given by

(D-14)
$$\frac{d^2T}{dx^2} = \frac{+Q}{kA} = \frac{+Q}{k\pi a^2}$$

where Q = q/(L-D). q is total heat input in BTU/hr, as before. In region 2, the applicable differential equation is (D-1), as before, and also the solution is given via (D-3);

$$T = \frac{qx}{k(\pi a^2)} + T_A \quad .$$

Integrating (D-14) once with respect to x, obtain

(D-15)
$$\frac{dT}{dx} = \frac{qx}{k\ \pi a^2\ (L-D)} + C_2 \quad .$$

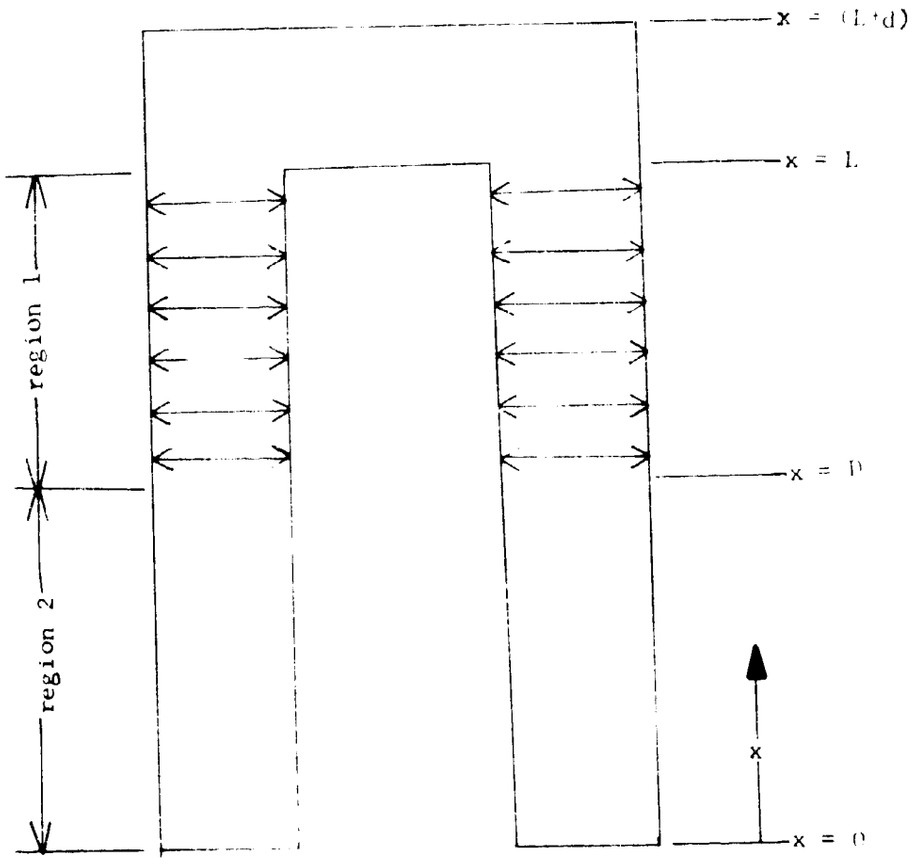

Figure D-3. Breakdown between center conductor and side walls of coaxial cavity.

The differential equation applicable in region 2, (D-1), may be substituted here to evaluate the arbitrary constant. At x = D

$$\frac{dT}{dx} = \frac{q}{k(\pi a^2)} = \frac{-qD}{k\pi a^2 (L-D)} + C_2 \tag{D-16}$$

from which

$$C_2 = \frac{-q}{k\pi a^2}\left[1 - \frac{D}{(L-D)}\right] \quad . \tag{D-17}$$

Now, integrating (D-15) a second time with respect to x, hence the relation

$$T = \frac{-q}{k\pi a^2 (L-D)} \frac{X^2}{2} + \frac{q}{k\pi a^2}\left[1 - \frac{D}{(L-D)}\right] X + C_3 \quad . \tag{D-18}$$

Evaluating the arbitrary constant C_3 by matching (D-18) with the solution in region 2 at x = D given by (D-3), the final result is

$$T = \frac{qD}{k(\pi a^2)} + T_A = \frac{-qD^2}{2k\pi a^2 (L-D)} + \frac{qD}{k\pi a^2}\left[1 - \frac{D}{(L-D)}\right] + C_3 \tag{D-19}$$

$$= \frac{-qD^2}{2k\pi a^2 (L-D)} + \frac{qD}{k\pi a^2} - \frac{qD^2}{k\pi a^2 (L-D)} + C_3 \quad ,$$

from which

$$C_3 = T_A + \frac{qD^2}{2k\pi a^2 (L-D)} \quad , \tag{D-20}$$

and in conclusion, the temperature distribution within region 1 is given by

$$T = \frac{qX^2}{2k\pi a^2 (L-D)} + \frac{q}{k\pi a^2}\left[1 - \frac{D}{(L-D)}\right] X + \left[T_A + \frac{qD^2}{2k\pi a^2 (L-D)}\right] . \tag{D-21}$$

A detailed analysis of this problem from this point on is difficult; however, a worst case analysis is arrived at by assuming a breakdown encompassing the entire center conductor (D = 0), for which

$$T = \frac{qX^2}{2k\pi a^2 L} + \frac{qX}{k\pi a^2} + T_A \quad . \tag{D-22}$$

Once again, the linear expansion of the center conductor due to heating is related to the coefficient of linear expansion via equation (D-4). Now proceed to numerically evaluate the thermal expansion of the center conductor due to heating, which is an indirect of the gaseous or multipacting type breakdown. A worst case estimate of expansion is found via

$$\Delta T = T - T_A = \frac{qL^2}{2k\pi a^2 L} + \frac{qL}{k\pi a^2} = \frac{qL}{2k\pi a^2} + \frac{qL}{k\pi a^2} \tag{D-23}$$

$$\Delta T = \frac{3}{2} \cdot \frac{qL}{k\pi a^2}$$

$$\Delta L = L \alpha \Delta T = \frac{1.5 \alpha q L^2}{k\pi a^2} \quad . \tag{D-24}$$

As before, center conductor length change can be related to the frequency by assuming the center conductor to be a quarter of a wavelength as the resonant frequency.

$$L + \frac{1.5 \alpha q L^2}{k\pi a^2} = \frac{\lambda}{4} \quad , \tag{D-25}$$

$$\frac{\lambda_o}{4} + \frac{1.5 \alpha q \lambda_o^2}{16\, k\pi a^2} = \frac{\lambda}{4} \quad , \tag{D-26}$$

from which

$$\frac{\lambda_o}{\lambda} = \frac{f}{fo} = \frac{1}{\left[1 + \frac{0.375 \alpha q \lambda_o}{k\pi a^2}\right]} \quad . \tag{D-27}$$

Using the handbook values of σ and k for aluminum as in case 1, (D-27) then is expressed

$$\frac{f}{fo} = \frac{1}{\left[1 + \frac{3.48\times10^{-8}\ q\ \lambda_o}{\pi a^2}\right]} \quad . \tag{D-28}$$

If λ_o and "a" are expressed in centimeters and "q" in watts

$$\frac{f}{fo} = \frac{1}{\left[1 + 3.62\times10^{-6}\ \frac{q\lambda_o}{\pi a^2}\right]} \quad . \tag{D-29}$$

Once again, it is convenient to characterize a breakdown in terms of breakdown power density P(watts/cm^2). But for this case, the area exposed to the breakdown is the side walls of the center conductor; hence,

$$A = 2\pi aL \tag{D-30}$$

$$\frac{f}{fo} = \frac{1}{\left[1 + 7.24\times10^{-6}\ \frac{P\lambda_o L}{a}\right]} \quad . \tag{D-31}$$

But assuming L is approximately a quarter wavelength

$$\frac{f}{fo} = \frac{1}{\left[1 + 1.81\times10^{-6}\ \frac{P\lambda_o^2}{a}\right]} \tag{D-32}$$

$$\frac{f}{fo} = \frac{1}{\left[1 + \frac{1.81\times10^{-6}\ P\lambda_o}{(a/\lambda_o)}\right]} \quad . \tag{D-33}$$

This shows that this breakdown condition is in a sense similar to the breakdown equation for case 1 given by (D-12); however, it is worsened by the inverse of (a/λ_o). It appears that making "a" large as possible minimizes the thermal effects of breakdown for this breakdown mode.

Specifically, to compare results of this breakdown mode with that of case 1, consider a VHF cavity (250 MHz). A wavelength is approximately 12[illegible] centimeters in which case

(D-34)
$$\frac{f}{fo} = \frac{1}{\left[1 + \frac{2.22 \times 10^{-4} P}{(a/\lambda_o)}\right]} \quad .$$

The results of the computation of frequency shift due to thermal heating for this case (case 2) are also plotted in figure D-2.

APPENDIX E

EXAMPLE DESIGN OF MULTICOUPLER CAVITY WITH MINIMUM SUSCEPTIBILITY TO CORONA MULTIPACTOR BREAKDOWN

As an example, a multicoupler shall be designed using the information in Section 5.0 and figure 5-1.

Since the information in figure 5-1 is straightforward, in this example figure 5-1 shall be changed to cover the general case. This is shown in figure E-1.

The following is an example of the use of Figure E-1.

Step A

Specify cavity power, Q_L, and frequency ; for example,

Power = 3 watts

Q_L = 100

frequency = 250 MHz .

Step B

Find a value of "a"

$$a = \left[\sqrt{\frac{3\ (100)\ (76.7)}{3035}} - 51\right]\lambda$$

a = 3.98 centimeters.

Step C

Is this value of "a" below TE_{11} cutoff and consistent with maximum allowable physical size ?

$$a_{te_{11}\ \text{cutoff}} = \frac{\lambda}{4.5\pi} = 8.5 \text{ centimeters.}$$

"a" is below TE_{11} cutoff, but assume the value of "a" computed in step B is not consistent with the maximum allowable physical size. Then proceed to step F.

Step F

Pick a highest practical value of "a" that is below TE_{11} cutoff and consistent with maximum allowable physical size. Assume mechanical constraints limit "a" to a value of 2 centimeters.

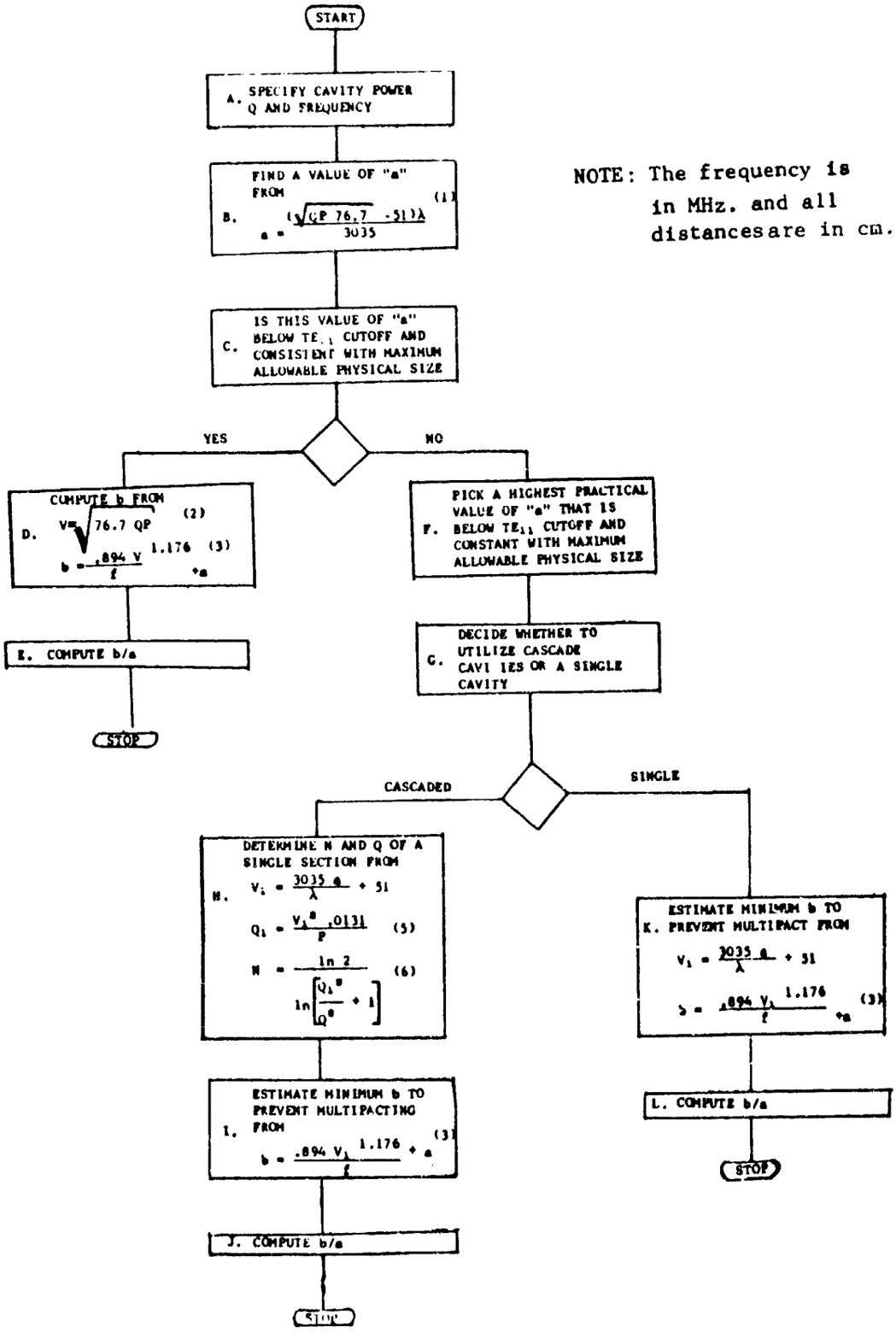

NOTE: The frequency is in MHz. and all distancesare in cm.

Figure E-1 Flow chart illustrating design procedures to eliminate corona and multipactor breakdown in multicouplers.

Step G

Decide whether to utilize cascade cavities or a single cavity. To decide this, try to use only a single cavity and see what it looks like.

Step K

Estimate minimum b to prevent multipaction

$$V_1 = \frac{3035(2)}{\lambda} + 51 = 101 \text{ volts}$$

$$b = \left(\frac{.894(101)}{250}\right)^{1.176} + 2 = 2.8193 \text{ centimeters} .$$

Step L

Compute b/a

$$b/a = \frac{2.819}{2} = 1.4$$

Since larger values of b can be used, giving larger b/a ratios, it may be desirable to use a b/a ratio of 3.65 (see figure 3-5) which will result in highest Q. Then

$b = (3.65)a = 7.30$ centimeter.

Note that the Q of this cavity is now (equation (5) in figure E-1):

$$Q = \frac{(101)^2 .0131}{3} = 44.7$$

By using cascaded cavities, the Q can be increased. Therefore, returning to Step G, the cascaded procedure will now be illustrated.

Step H

Determine N and Q of a single section

$V = 101$ volts

$$Q_1 = \frac{(101)^2 (.0131)}{3} = 44.7$$

$$N = \frac{\ln 2}{\ln\left[\frac{(44.7)^2}{(100)^2} + 1\right]} = 3.7 \Longrightarrow 4 .$$

The required number of cavities is found to be 4. If a lower value of Q_1 can be tolerated, fewer cavities can be used.

Step I

Determine minimum b to prevent multipacting.

$$b = \frac{.894\ (101)^{1.176}}{250} + 2 = 2.8193 \text{ centimeters} .$$

Step J

Compute b/a

$$b/a = \frac{2.819}{2} = 1.4$$

If desired to increase the b/a ratio to 3.65 for optimum Q, then b is increased to

$$b = 3.65\ a = 7.3 \text{ centimeters} .$$